

THESIS FOR THE DEGREE OF DOCTOR OF PHILOSOPHY IN  
NATURAL SCIENCE, SPECIALIZING IN CHEMISTRY

# Salting-out of Colloidal Latex Particles Grafted with Poly(ethylene glycol)

G. Kristin Jonsson



UNIVERSITY OF GOTHENBURG  
Department of Chemistry and Molecular Biology  
Gothenburg, Sweden, 2020

ISBN 978-91-629-0353-4 (Print)  
<http://hdl.handle.net/2077/62711> (PDF)

Printed by BrandFactory  
Gothenburg, Sweden, 2020

Typeset in L<sup>A</sup>T<sub>E</sub>X

Parts of this thesis are from the author's Licentiate dissertation "Stability of Sterically Stabilized Monodispersed Fluorinated Spheres" which was presented on the 11<sup>th</sup> of December 2017.

# List of Papers

This thesis is based on the following papers which will be referred to in the text by their Roman numerals. The papers are reproduced with permission from the journals when necessary.

**Paper I Semi-batch synthesis of colloidal spheres with fluorinated cores and varying grafts of poly(ethylene glycol)**

G. Kristin Jonsson, Jeanette Ulama, Malin Johansson,  
Malin Zackrisson Oskolkova and Johan Bergenholtz  
*Colloid and Polymer Science*, **295**(10), 1983-1991, 2017.

**Paper II Stabilizing Colloidal Particles against Salting-out by Shortening Surface Grafts**

G. Kristin Jonsson, Jeanette Ulama, Rasmus A. X. Persson, Malin Zackrisson Oskolkova, Michael Sztucki, Theyencheri Narayanan and Johan Bergenholtz  
*Langmuir*, **35**(36), 11836-11842, 2019.

**Paper III Effect of salting-out on the interfacial activity of colloidal particles stabilized by poly(ethylene glycol)**

G. Kristin Jonsson, Malin Johansson, Grethe Vestergaard Jensen, Michael L. Davidson, Lynn M. Walker, Romain Bordes and Johan Bergenholtz  
*Submitted to Journal of Colloid and Interface Science*

**Paper IV Colloidal cluster formation caused by salting-out of polymer-grafted particles**

Johan Bergenholtz, G. Kristin Jonsson  
*Manuscript*

# Contribution Report

- Paper I** I performed the syntheses of the particles grafted with mPEGA polymers of 5000 g/mol, as well as the particles with a polystyrene core. I performed the SAXS analysis, the DCP measurements of the former as well as the DLS measurements of both the former and latter. In addition, I did the cryo-EM image analysis and contributed to the discussion around it. I also wrote the “Crosslinked particles” section of the paper and part of the “Conclusions”.
- Paper II** I performed all of the synthesis work. I carried out the SAXS measurements with technical assistance and I analyzed some of the SAXS data using model fitting. I performed the DLS stability measurements of the new batches as well as for the LL25 batch. I wrote everything, except the part about the Flory-Huggins model for the stability, in a first draft of the paper. I contributed to the development of the Flory-Huggins model.
- Paper III** I performed the synthesis, the majority of experimental planning, execution and interpretation of the results as well as most of the measurements, exception being the non-dialyzed particles in the pendant drop method and the Pickering emulsions. The SANS measurements were done with assistance. In addition, I wrote the first draft of the paper.
- Paper IV** I performed the synthesis as well as all the sample preparations. I did the SAXS measurements together with the co-author with on-site technical assistance at the ESRF.

# Abstract

Colloidal particles dispersed in a medium are important both in nature and in industry. The stability of colloidal particles is determined by the interactions between them and can be improved by steric stabilization. There is no conclusive understanding of how these sterically stabilized particles become unstable. In order to understand the loss of repulsion that leads to instability, model systems of well-defined dispersions are needed.

A semi-batch emulsion polymerization scheme has been used in this work in order to yield highly monodisperse, spherical core-shell particles in an aqueous medium. The cores of the particles are fluorinated, resulting in a refractive index close to that of water. By having the particles almost refractive index-matched, the core-core van der Waals attractions are minimized. This makes it possible to study the role of the grafted polymers.

In order to test the versatility of the synthesis scheme, crosslinked particles and particles with a polystyrene core, instead of the fluorinated core, have been synthesized. Moreover, syntheses with different lengths of the grafted polymer, yielding different thicknesses of the particle shell, have been performed. The stability of the colloids with respect to the addition of sodium carbonate has been tested. The results show that the particles with the shortest grafts are the most stable ones. For longer grafts, the stability limit, in terms of added salt, levels out. These experimental results have been fitted to a Flory-Huggins based model.

Both small-angle X-ray and neutron scattering (SAXS and SANS, respectively) measurements were performed on the particle dispersions employing two different kinds of salt in a range of concentrations. The SAXS measurements showed that the stability limit was independent of the particle concentration. This was explained by salt-induced, single-particle dewetting being the driving force for permanent aggregates to form. To investigate this hypothesis, the PEG layer was made more visible in the SANS measurements by changing the solvent to a  $\text{H}_2\text{O}:\text{D}_2\text{O}$  mixture. A decrease in the shell thickness was observed at salt concentrations close to where the particles start to aggregate, in support of the hypothesis. Also, at this point a peak at large scattering angles, corresponding roughly to the same length scale as the layer thickness, disappears in the SAXS measurements.

Moreover, dewetting of the PEG-layer was also indicated through structure determination, of the clusters formed in unstable dispersions, from SAXS mea-

surements and computer calculations of the structure factor. The distance of closest approach of two particles in the clusters is smaller at higher salt concentrations, which could be explained by the grafted polymer layer contracting.

To further investigate the dewetting of the PEG-shell, interfacial tension (IFT) measurements were performed between aqueous dispersions with varying salt concentrations and toluene. A decrease of the IFT showed that the particles are surface active, even without salt. However, the IFT decreased more strongly in the presence of salt. A strengthening of the surface activity on adding salt supports the dewetting hypothesis.

# Summary in Swedish

Kolloidala partiklar dispergerade i ett medium är viktiga både industriellt och i naturen. Stabiliteten för dessa kolloidala system beror på interaktionerna mellan partiklarna och kan förbättras genom sterisk stabilisering. Det finns ingen entydig teori om vad som avgör stabiliteten för steriskt stabiliserade partiklar och framför allt saknas kunskap om vad som orsakar destabilisering. För att kunna avgöra vad som leder till instabilitet och aggregation i sådana system så behövs ett väldefinierat modellsystem.

I det här arbetet har fluorinerade sfäriska “*core-shell*”-partiklar syntetiserats via en “*semi-batch*”-emulsionspolymerisering i vatten. Partiklarna är steriskt stabiliserade genom att polymeren polyetylenglykol (PEG) är kemiskt bunden vid ytan. Då partiklarna har en fluorinerad kärna får de ett brytningsindex som är nära dispersionsmediets. Genom att partiklarna och dispersionsmediet är nästan helt brytningsindexmatchade så minimeras van der Waals-växelverkan mellan partikelkärnorna. Detta gör det möjligt att undersöka effekten som de bundna polyetylenglykolkedjorna har på stabiliteten.

Flera olika längder på polyetylenglykolkedjan har använts i olika synteser. Förutom det har även synteser gjorts där mångsidigheten hos syntesupplägget ytterligare testats genom att tvärbinda partiklarna samt använda polystyren som kärna istället för den fluorinerade kärnan. Stabiliteten vid tillsats av natriumkarbonat har undersökts och resultaten visar att ju kortare polyetylenglykolkedja partiklarna har som skal, desto högre koncentrationer av natriumkarbonat krävs för att göra dem instabila. Partiklarna med de allra kortaste polyetylenglykolkedjorna har inte gått att destabilisera. De olika stabilitetsgränserna uttryckta som koncentration natriumkarbonat har anpassats till en ekvation baserad på Flory-Huggins-parametern.

Vidare har röntgenspridningsmätningar visat att stabilitetsgränsen för partikeldispersionerna inte påverkas av partikelkoncentrationen. Detta förklaras genom saltpåkallad enpartikelavvattning som drivkraften för bildandet av permanenta aggregat. För att undersöka den här hypotesen, synliggjordes PEG-lagret tydligare i neutronspridningsexperiment genom att byta lösningsmedel till en  $H_2O:D_2O$ -blandning. Genom dessa mätningar visades att nära stabilitetsgränsen kontraherar lagret, till stöd för avvattningshypotesen. Dessutom försvinner en topp uppmätt vid stora spridningsvinklar, motsvarande ungefär samma längdskala som lagrets tjocklek, i SAXS-mätningarna vid höga saltkoncentrationer.

Avvattning av PEG-lagret indikerades även genom strukturbestämning av kluster, som bildas i instabila dispersioner, från SAXS-mätningar och datorberäkningar av strukturfaktorn. Avståndet mellan två närliggande partiklar i klustret är mindre vid högre saltkoncentrationer, vilket skulle kunna förklaras av att lagret kontraherar.

Gränsytspänningsmätningar genomfördes mellan partikeldispersion med salt och toluen. Resultaten visar en minskning i gränsytspänningen även utan salt men en större minskning med salt i vattenfasen. Detta visade att partiklarna ansamlas spontant vid vatten-toluengränsytan men drivs dit till en högre grad i närvaro av salt. Detta stödjer avvattningshypotesen.

# Contents

<b>Abstract</b>	<b>i</b>
<b>Summary in Swedish</b>	<b>iii</b>
<b>Contents</b>	<b>v</b>
<b>1 Introduction</b>	<b>1</b>
1.1 Purpose . . . . .	3
1.2 Thesis outline . . . . .	3
<b>2 Background</b>	<b>5</b>
2.1 Poly(ethylene glycol) . . . . .	5
Phase behavior . . . . .	5
Salting-out . . . . .	6
2.2 Emulsion polymerization . . . . .	6
2.3 Colloidal interactions . . . . .	8
van der Waals forces . . . . .	8
Double layer repulsion . . . . .	9
DLVO theory . . . . .	9
Steric force . . . . .	10
2.4 Surface active particles . . . . .	11
<b>3 Methods</b>	<b>15</b>
3.1 Dynamic light scattering . . . . .	15
3.2 Small-angle scattering . . . . .	16
3.3 Cryo-electron microscopy . . . . .	18
3.4 Differential centrifugal photosedimentometry . . . . .	19
3.5 Pendant drop method . . . . .	20
3.6 Synthesis and sample treatment . . . . .	22
Chemicals and pre-treatment . . . . .	22
Experimental set-up and execution . . . . .	22
Post-treatment of dispersions . . . . .	24
3.7 Scattering models with structure factor . . . . .	25
<b>4 Results</b>	<b>27</b>

CONTENTS

---

4.1	Paper I . . . . .	27
4.2	Paper II . . . . .	29
4.3	Paper III . . . . .	34
4.4	Paper IV . . . . .	39
<b>5</b>	<b>Conclusions and future work</b>	<b>43</b>
	<b>Bibliography</b>	<b>47</b>

# Chapter 1

## Introduction

The milk we drink, the paint we use on our house, the ice cream we enjoy and the blood pumping through our veins are all examples of colloidal systems, also commonly called colloidal dispersions. Indeed, colloidal dispersions are highly present in our daily life and occur in a wide range of apparently very different systems. What all these different systems have in common is that there is a discontinuous phase (“particles”) of submicron size, which is more or less evenly distributed in a continuous phase.

The colloidal systems that exist naturally, or those produced industrially, are often composed of many components and understanding the behavior of such dispersions becomes complicated. Therefore, there is a need for well-defined, monodisperse colloidal dispersions that can be more easily studied. The academic research on such model systems, as well as on their synthesis, is comprehensive. Colloidal dispersions, with a narrow size distribution, well-defined interactions and particles of spherical shape, can be used to study a number of phenomena. Some examples are the glass transition or the crystal nucleation of hard spheres. For instance, poly(methylmethacrylate) and silica particles in organic solvents have been used to study glass formation and other aspects related to phase behavior of hard spheres and attractive spheres [1, 2, 3, 4]. Polystyrene and fluorinated sphere systems have been employed to understand the effect of long-range repulsion on static and dynamic [5, 6] properties, and also crystal formation [7]. Colloidal dispersions can also, to some extent, act as model systems for atoms and molecules [1]. The colloids are in most cases easier to study since they are of sizes comparable to the length scales of visible light. This opens up for techniques such as optical experiments, like microscopy and light scattering.

The stability of a colloidal system is crucial for its technological use. Often, colloidal systems can be stabilized electrostatically. However, this is not generally possible when the solvent is non-polar or in media of high ionic strength. In this case, one common way of stabilizing colloidal systems is by either chemically grafting or physically adsorbing polymers onto the particle surface, leading to so-called steric stabilization. Moreover, there are other advantages with ster-

ically stabilized particles, such as reasonable redispersibility once aggregated, frozen or dried. Despite the importance of these systems, the understanding of steric stabilization is both scattered and incomplete [8, 9, 10, 11], particularly in the transition region up to their becoming unstable.

Some examples of parameters which influence the stability of polymer coated particles are the interactions of polymer and solvent, often taken to be sufficiently well described by the so-called solvent quality [12], the grafting density of the polymer chains [13, 14, 15], and the core-core London-van der Waals (vdW) forces [16]. One model for the steric stabilization explains the repulsion by the decrease of entropy due to steric interpenetration of the grafted polymers [12] but for other systems it is enthalpically controlled. In the former, the system becomes unstable as the temperature is lowered, whereas for the latter the opposite trend holds. Another model was proposed by Kramb and Zukoski [17] where, in a poor solvent, the grafted polymer contracts exposing a core-core vdW attraction. Another model calls on Lifshitz theory and asserts that the refractive index of the overall particle is increased when a polymer shell contracts in poor solvent. The increase in refractive index thereby leads to an increase in vdW attraction between the particles [18]. Yet another model, based on experiments on non-aqueous systems, ascribes instabilities to an ordering transition in the polymer graft [19, 20]. Thus, there is far from any consensus regarding the mechanism responsible for polymer-grafted particles losing their stability.

Recently, Vaknin and coworkers examined yet another possible explanation for the instability of PEG-grafted gold nanoparticles in a number of papers [21, 22, 23, 24]. They discovered that the polymer-grafted gold nanoparticles were surface active, spontaneously creating a monolayer at the air-water surface. Upon adding salt the particles at the interface go from a random ordering (no salt) to a lattice. They argue that the instability is due to competition for the water molecules between added electrolyte and the PEG chains, i.e. the PEG chains are “salted out”. This means, that the PEG goes from a wetted to a dewetted state to escape the solvent but the grafted PEG chains intertwine with those of neighbouring particles rather than contracting on the same particle. Hence, the particle aggregate. The type of salt is important as some ions are known, according to the Hofmeister series, to be better at precipitating (by making the solvent “poor”) proteins and other colloids from solution [25].

In this work, core-shell particles have been synthesized and studied. For these the core-core vdW forces are minimized by having the index of refraction of the particle cores close to that of the solvent [26], in this way making the influence of the grafted polymer more pronounced. With such a model system, it is anticipated that one should be able to discriminate between the various models for the mechanism by which particles become unstable. For instance, the model proposed by Kramb and Zukoski [17] should not be applicable at all in the absence of a net vdW attraction between particles. The particle core is composed of heptafluorobutyl methacrylate (HFBMA) polymer and the shell of poly(ethylene glycol) polymers with acrylate and methoxy end groups (mPEGA). Furthermore, the particles are considerably larger than the gold nanoparticles studied by Vaknin and coworkers [21, 22, 23, 24] resulting in

a PEG-shell that is a much smaller part of the overall core-shell particle. The solvent condition is worsened by adding salt, in the present case mainly sodium carbonate. The carbonate ion is one of the strongest “salting-out anions”, according to the Hofmeister series [27], binding water molecules tightly. The goal is to remove much of the core-core vdW attraction so that the role of the polymer can be clearly elucidated. In order to understand the effect of polymer chain length on the stability, several different PEG molecular weights have been used in the synthesis resulting in different shell thicknesses. The dispersions, containing particles with different PEG-shell thicknesses, have been studied in varying amounts of salt using mainly small-angle scattering (neutron and X-ray) and dynamic light scattering. In addition, the interfacial tension between dispersions, at various salt concentrations, and toluene has been investigated.

## 1.1 Purpose

The purpose of this work is to study polymeric stabilization, when going from good solvent conditions to poor solvent conditions, to determine the mechanism behind how steric stability is lost. In addition, the role of the chain length, pivotal in many models, is to be clarified. Also, the nature of the transition to the aggregated state is to be clarified, such as whether it is more akin to reversible flocculation, as widely believed, or to irreversible coagulation.

## 1.2 Thesis outline

This work is presented as follows: The background information, giving an overview of the important foundation for this work is provided in Chapter 2. It starts out with a discussion on the versatile PEG polymer that has been used in this work as a steric stabilizer. Emulsion polymerization is then covered, followed by a brief description of different colloidal interactions, and, lastly surface active particles. The methodology is described in Chapter 3, providing an overview of the main experimental techniques that have been used in this work, as well as the synthesis of the monodisperse particles. The experimental results are presented in Chapter 4. These are mainly based on four research articles that are appended to the end. Finally, the main conclusions are summarized and possible future work is discussed in Chapter 5.



## Chapter 2

# Background

### 2.1 Poly(ethylene glycol)

Poly(ethylene glycol) (PEG) is a versatile polymer molecule that is commercially available in both linear and branched forms and in many different molecular weights (MW). PEG is also known as poly(ethylene oxide) (PEO), poly(oxyethylene) (POE), and polyoxirane. Usually, the name “PEO” is used when the MW is above  $\sim 20,000$  g/mol and “PEG” below this value. There is no clear rule for when “POE” and “polyoxirane” are used [28]. In this work, low MWs are used and only variations of the name “PEG” will be employed to avoid ambiguity, even when discussing other studies with high MW polymers. PEG is widely used in technological applications. One important example is its use to prolong circulation times in vivo in the context of drug delivery [29].

#### Phase behavior

PEG exhibits an unusual property in that it is soluble both in water and a number of organic solvents [28]. In fact, PEG has experimentally been shown to be surface active [30, 31] as well as interfacially active [32]. Ito et al [32] found that high-MW PEG had the same affinity for the interface between toluene and water, regardless of in which phase the PEG was initially dispersed. The end group and the MW of PEG both affect the surface activity [33], at least for a MW below 3000 g/mol, above which the type of end group becomes less important. Having methyl-terminated PEG, in contrast to the more commonly hydroxyl-termination, increases the hydrophobicity due to less opportunities for hydrogen bonds with the water molecules [33, 34]. It is noticeable that the end group for low-MW PEG becomes more important when the solvent quality is decreased [34].

In aqueous media, PEG will form a two-phase system under certain conditions, such as when changing the temperature or adding a salt. Both a lower and an upper critical solution temperature are found for PEG in water, forming a “closed loop”-type phase diagram at elevated temperatures. The upper and lower critical temperatures are found to depend on the MW [35].

## Salting-out

Adding salt to an aqueous solution containing PEG will, depending on the type of salt, lead to a two-phase system. Several inorganic salts have this property [36] and they differ by the concentration needed for this phase separation. High-valence ions are generally better salting-out agents than low-valence ones. However, also the type of ion and not only its valency affects its salting-out efficiency. Indeed, the salting-out efficiency of an ion is not completely captured by any classical theoretical model [27]. This is especially true for anions.

The salt concentration at which this phase separation takes place decreases as the PEG concentration increases. A theoretical model for this salt dependence of the PEG solubility has been proposed by Florin et al. [37]. In their work, they suggest that close to the PEG chains, there is depletion of ions. It is then the overlap of these depletion zones that causes the PEG-PEG attractions leading to phase separation. The ion-specificity is caused by preferential solvation of ions, leaving PEG dehydrated to varying extent at a given salt concentration. Frank and Evans [38] categorize ions into “structure makers” and “structure breakers” depending on their tendency for preferential solvation. Structure makers, such as  $F^-$ ,  $CO_3^{2-}$  and  $SO_4^{2-}$ , usually have a high charge density and are strongly hydrated. These are also known as kosmotropes, and salting-out agents according to the Hofmeister series. Structure breakers are characterized by low charge density and weaker interactions with water. The tie lines in the PEG-electrolyte phase diagram show that a PEG-rich phase with little salt coexists with a PEG-poor phase enriched with salt, i.e. a demixing-type phase transition.

## 2.2 Emulsion polymerization

Emulsion polymerization is a widely used synthesis technique both in industry and academia [39], because of the flexibility of the synthesis and therefore also of the end product. There is no conclusive theory of the mechanism at work in emulsion polymerization and several models have been proposed. Harkins [40, 41, 42, 43] gave a qualitative explanation for emulsion polymerization, and his model became the starting point for several researchers who have continued the development, *e.g.* Smith and Ewart (SE) [44, 45, 46]. In these, the formation of micelles via surfactants is central. They therefore fail to explain how particles are formed when no micelles are present or when monomers are water soluble.

Another model explaining the emulsion polymerization is the HUFT (after Hansen, Ugelstad, Fitch and Tsai) theory [47, 48], also known as the homogeneous nucleation model. In contrast to the Harkins/SE theory, the HUFT model explains emulsion polymerization without the need for micelles. The radicals react in the solvent medium with the monomer, forming oligomers. Particles are formed when the oligomers reach a critical length for which they are not soluble anymore.

The extent to which the synthesis in this work follows the micellar or homogeneous nucleation model is beyond the scope of this work. Presumably it

contains features of both in that the PEG macromonomer is water soluble but becomes amphiphilic after reaction with fluorinated monomer. The degree of amphiphilicity will vary with the molecular weight of the macromonomer.

To make the situation even more complicated, emulsion polymerization can be carried out in different manners. All of the reactants can be added all at once or throughout the synthesis. In semi-batch (or semi-continuous) polymerization, one of the chemicals, usually the monomer, is added throughout the synthesis (either continuously or in increments) [49].

In this work, core-shell particles were synthesized with a fluorinated core grafted with a reactive heterobifunctional PEG macromonomer, methoxy-PEG acrylate (mPEGA). Syntheses of fluorinated particles have been reported earlier. Härtl et al. [50] and Pan et al. [51] managed to produce highly charged fluorinated polymer particles by an aqueous emulsion polymerization of fluorinated alkyl acrylate monomers. Härtl et al. found that by varying the monomer concentration or the stirring rate in the synthesis, they were able to control the particle size. However, Koenderink et al. [52] found that following Härtl's synthesis protocol did not yield monodisperse particles. In order to achieve this, they changed the reaction conditions, using higher monomer concentrations and higher temperatures. Like Härtl et al. [50], the size of the particles could be controlled by changing the monomer concentration.

In order to obtain larger particles than was possible by regular emulsion polymerization, Koenderink et al. [52] used a seeded emulsion polymerization scheme. They also synthesized core-shell particles with a fluorinated shell using this seeded emulsion polymerization protocol, albeit with some loss of monodispersity which they could correct post-synthesis. The work of Koenderink et al. [52] was extended by Sacanna et al. [53], who synthesized smaller (17-50 nm) fluorinated particles using microemulsions.

Suresh et al. [54] also managed to produce fluorinated core-shell particles by seeded emulsion polymerization. In their work, they used a semi-batch approach adding the second monomer slowly throughout the synthesis. The particle growth during the synthesis, microstructure of the particles, the film morphology and mechanical properties were studied.

Copolymerizing the fluorinated monomer with mPEGA macromonomers is challenging. However, highly monodisperse particles are necessary in this work which has therefore required a different synthesis route. It has been found that a version of the semi-batch emulsion polymerization scheme, using HFBMA as monomer and grafting with mPEGA, initiated by potassium persulfate (KPS), yields highly monodisperse core-shell particles [26]. In order to reach a high degree of monodispersity, the initiator, instead of the monomer, has been added continuously for the first couple of hours of the reaction. The syntheses have been performed with a wide range of shell layer thicknesses by using different MW mPEGA.

## 2.3 Colloidal interactions

### van der Waals forces

The literature on van der Waals (vdW) forces is voluminous. Here follows a short introduction to the subject with emphasis on the mechanisms most important to the work in this thesis.

vdW forces are relatively long-ranged forces that derive from the short-range molecular interactions acting in concert. In the Hamaker pairwise additive theory, they can be expressed as the sum of the molecular Keesom, Debye and London dispersion (LD) forces, *i.e.*

$$\mathbf{F}_{\text{vdW}} = \mathbf{F}_{\text{Keesom}} + \mathbf{F}_{\text{Debye}} + \mathbf{F}_{\text{LD}}$$

The Keesom and Debye forces are due to electrostatic interactions involving molecules that are polar. More specifically, the Keesom energy is due to dipole–dipole interactions between freely rotating molecules [55, 56]. The dipole–dipole force can be either attractive or repulsive depending on how the dipoles are oriented, but in equilibrium the dipoles will tend to align and attract each other. The Debye force is due to interactions between a polar molecule which is free to rotate and a non-polar molecule [57]. The polar molecule polarizes the non-polar molecule, leading to a dipole–induced dipole interaction, which always leads to an attraction.

Unlike the Keesom and Debye forces, the third component of the vdW force, the LD force, is always present between molecules, even for neutral, non-polar ones. In many colloidal systems, the LD forces are also the largest contribution to the total vdW force [58]. While the former two components of the vdW force are quite straightforward to understand and model, the LD force cannot be simply described by classical physics. Instead, quantum mechanical perturbation theory must be used. The London dispersion force has its origin in the fact that even non-polar molecules may have an instantaneous dipole moment because the electrons not being always symmetrically positioned around the nuclei. This microscopic explanation was developed by Fritz London [59, 60] in the 1930s.

Hamaker [61] summed the molecular forces in a pairwise fashion and obtained a force law that depends on the geometry as well as on the materials involved. The latter appears through the so-called Hamaker constant, which is often taken as an empirical constant to describe the strength of the interaction. Hamaker assumes that the interactions between two colloidal particles can be summed independently over all of the molecules. In this assumption, neighboring molecules do not affect each other. This is an approximation but Lifshitz developed a theory for Hamaker’s constant without resorting to pairwise additivity. In the Lifshitz theory the material properties are described via frequency-dependent dielectric functions. The geometry cannot be decoupled from the material properties, except for the case of flat plates.

In the case where two identical phases interact across a medium the Hamaker

constant (A) is, according to the Lifshitz theory [61], given approximately by

$$A = \frac{3}{4}kT \left( \frac{\varepsilon_1 - \varepsilon_3}{\varepsilon_1 + \varepsilon_3} \right)^2 + \frac{3hv_e}{16\sqrt{2}} \frac{(n_1^2 - n_3^2)^2}{(n_1^2 + n_3^2)^{3/2}} \quad (2.1)$$

where  $\varepsilon$  is the relative permittivity,  $n$  is the refractive index,  $v_e$  is the main electronic absorption frequency in the UV-region, and  $h$  is Planck's constant. The first term in equation 2.1 is often interpreted as the Keesom and Debye forces [57] but it has also some quantum mechanical character [62]. The second term, representing the LD force, is usually the dominant contribution to the Lifshitz-Hamaker constant [57] but it disappears if the refractive index of the particles ( $n_1$ ) equals the refractive index of the solvent ( $n_3$ ). In addition, the first term in equation 2.1, being mostly electrostatic in nature, is thought to be diminished by added electrolyte via screening [63].

### Double layer repulsion

Colloidal particles which are dispersed in a polar solvent, such as water, are often electrically charged. The surface charge for such systems is brought about by mainly two different mechanisms [61]: i) ionization of surface groups, by for instance dissociation or protonation, or ii) adsorption of ions from the liquid medium onto the surface.

The overall system must maintain a zero net charge. This means that an equal amount of charge, opposite in sign to the surface charge and typically carried by ions dispersed in the solution, is present. These ions are called counterions. In the solution there will also be ions which carry the same charge as the surface. They are called co-ions. Figure 2.1 provides an illustration of the ions that make up a so-called "diffuse double layer" outside the colloid surface. The counterions will be in excess close to the surface. Far from the surface there will be as many counterions as co-ions.

The charges in the diffuse double layer create an electrostatic potential. The forces on these ions are given by the derivative of this electrostatic potential with respect to position. By calculating the electrostatic potential, and the concentration of counterions and co-ions, at each point in the system, one can calculate the force between two charged surfaces with double layers [64]. The calculation of both the electrostatic potential and the distribution of ions is complicated and approximations are invariably introduced. This force is in most cases repulsive when charged surfaces have the same sign [62] and the range of the repulsion decreases with increasing ion concentration, which is a phenomenon known as screening.

### DLVO theory

The DLVO theory (named after the scientists Derjaguin, Landau, Verwey and Overbeek) takes the total interaction to be the sum of the vdW forces and the double layer repulsion. The DLVO theory is a cornerstone of colloidal science. It

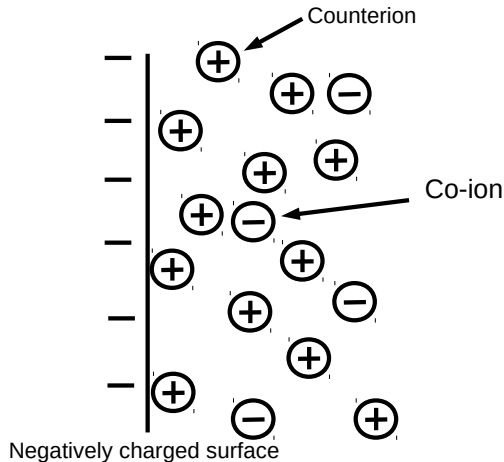


Figure 2.1: Schematic representation of the diffuse double layer.

captures semi-quantitatively the stability behavior of aqueous colloidal dispersions, including the empirical Schulze-Hardy rule. The DLVO theory has some shortcomings however. Among these is the inability to describe very short-range interactions and specific ion effects. The former is often referred to as the hydration force and its effect is related to the organization of the water molecules close to a surface [65]. While the origin of the hydration force is attributed to the change in organization of water molecules, there is an uncertainty in how this occurs at a molecular level. Several theoretical models have been proposed [66, 67, 68, 69, 70] but so far no consensus has been reached. The latter refers to the fact that the behavior is not only determined by the valence of ions but also their chemical identity.

### Steric force

Colloidal particles that are not normally stable in a solvent can be sterically stabilized, sometimes by simply adding a polymer additive. The polymer might either be grafted irreversibly or physically adsorbed on the particle surface.

Steric stabilization forces are not well understood. There is no comprehensive theory, and perhaps even less understood is why dispersions can be destabilized by poor solvent conditions. One possible model for why this occurs was proposed by Napper [71] and is illustrated in figure 2.2. In a good solvent, the polymer chains of the outer layer move relatively freely and have high entropy. When two particles come in contact with each other, the chains become entangled and lose entropy. This leads to a repulsion. However, in a poor solvent, brought on by lowering the temperature, this entropic mechanism

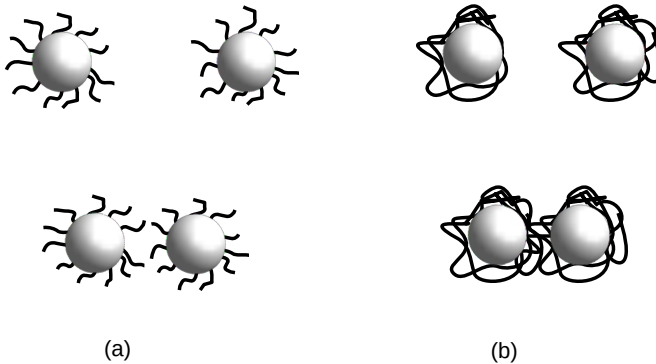


Figure 2.2: Illustration of core-shell particles in a good (a) and poor (b) solvent at long (upper) and short (lower) distance according to Napper [71]. In the poor solvent the shell has collapsed and to further decrease the shell-solvent contact the particles aggregate. In the good solvent, the outer polymer shell has high entropy which results in a repulsion at close distances between two particles.

becomes increasingly less important. Moreover, if the solvent is poor, the chains will collapse to avoid the solvent and so their entropy is low and cannot decrease further.

Another possible model is that when the outer layer collapses in a poor solvent, the core-core vdW attractions become exposed and the particles attract each other. In figure 2.3 the core-core attraction energy is shown, schematically, as a function of distance between the particles. As the distance is decreased, an attraction develops up until the point where they cannot approach any closer. Kramb and Zukoski [17] suggest that the outer polymer layer keeps the depth of the interaction energy shallow by preventing particles from sampling the core-core vdW attractions. This effect stabilizes the grafted particles in a good solvent (case (a) in figure 2.3). However, in a poor solvent the layer contracts or even collapses and the vdW core-core attraction becomes exposed rendering the particles unstable (case (b) in figure 2.3).

## 2.4 Surface active particles

Nano- and microparticles may act in a similar manner to surfactant molecules as to regards surface activity. However, surface-active particles do not have the ability to form micelles but they aggregate at sufficiently high concentrations. One way in which they resemble surfactant molecules is when stabilizing emulsions. However, particles that are weakly unstable are better stabilizers of

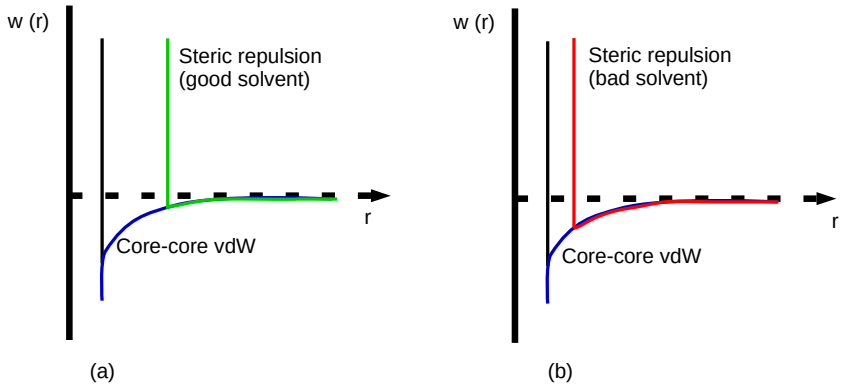


Figure 2.3: Schematic graph of the core-core vdW attraction between two particles. Black and blue lines in both case (a) and (b) represent colloids without a shell. The green line in (a) shows the net interaction, in a good solvent, between two particles which exhibit an outer shell. In (b) the core-shell particles are in a bad solvent.

emulsions [72, 73, 74], often better than surfactant molecules, and they can also produce so-called “multiple emulsions” (emulsions inside emulsions) [74].

In contrast to amphiphilic molecules, where the hydrophilic/lipophilic properties primarily decide the formation and stability of emulsions, the situation is more complicated for surface-active particles [74]. The reason the surface-active particles reside at the interface of two fluids is the decrease in free energy due to a decreased area of contact between the two fluids which lowers the macroscopic interfacial tension. In fact, if the particles are small enough, so that gravity does not need to be taken into account, the free energy required to remove a particle from a water-oil interface,  $-\Delta_{\text{int}}G$ , is given by

$$-\Delta_{\text{int}}G = \pi r^2 \gamma_{\text{ow}} (1 \pm \cos \theta_{\text{ow}})^2, \quad (2.2)$$

where  $r$  is the particle radius,  $\theta$  is the angle the particle makes with the interface measured in the water phase (see figure 2.4), and  $\gamma_{\text{ow}}$  is the interfacial tension between water and oil. (The cosine is negative when the particle is removed from the interface into the water phase and positive when it is removed into the oil.) From this equation, it is obvious that both the angle (i.e. the wettability of the particles) and the size of the particles, play a crucial role in how well they stabilize emulsions. Smaller particles will have a smaller  $|\Delta_{\text{int}}G|$  and therefore will not stabilize the emulsion as efficiently as larger ones.

Not only does the wettability of the particle affect the stability of the emulsion, but also the type of emulsion formed. Particles with low wettability

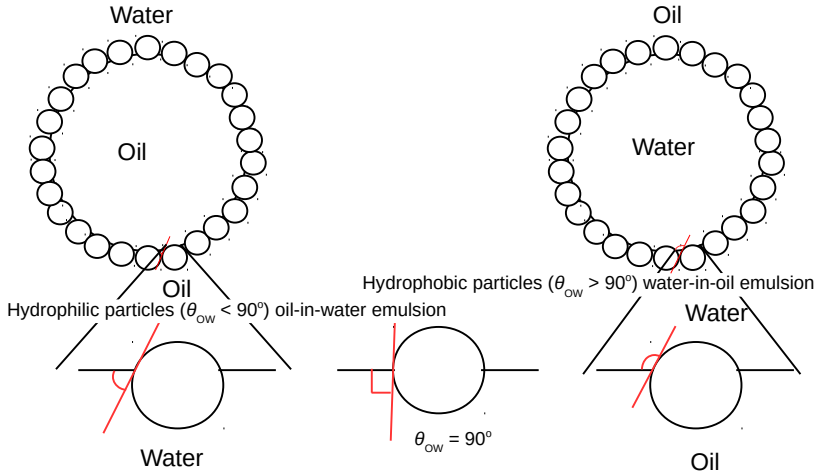


Figure 2.4: Schematic representation of oil-in-water and water-in-oil emulsions as stabilized by particles with different contact angles. Depending on the wetting properties of the particle, oil-in-water emulsions (left) or water-in-oil emulsions (right) are formed.

( $\theta > 90^\circ$ ) will be mostly in oil and create water-in-oil emulsions since this allows a larger part of the particle to reside on the convex side of the emulsion droplet. In contrast, hydrophilic particles that will be wetted by the water phase, will have contact angles below  $90^\circ$  and produce oil-in-water emulsions. As seen in figure 2.4, the contact angle is directly related to the interfacial area covered by the particle. This is the area excluded from contact between the two fluids and it is maximized at  $\theta = 90^\circ$ . Consequently, the greatest stability is obtained with particles that are equally hydrophobic and hydrophilic.

One common way of stabilizing particles is by grafting polymers to their surface. However, equation 2.2 does not take into account any effects of polymer grafts. Isa et al [75] have developed a model for polymer-brush-grafted particles at the interface. The extent of the grafts depends on the solvent quality, in their work calculated by the Flory-Huggins theory. As the solvent quality is worsened, the brush contracts to avoid contact with the solvent molecules. This contraction of the layer decreases the area covered by the particle at the interface (see figure 2.5), which leads to a decrease in the lowering of the interfacial energy provided by the particle. At the same time, the second solvent becomes relatively better for the polymer brush and the particle moves toward it. Assuming that it is the good solvent that is worsened, this leads to an increase of the area covered at the interface. The resulting effect depends on many parameters.

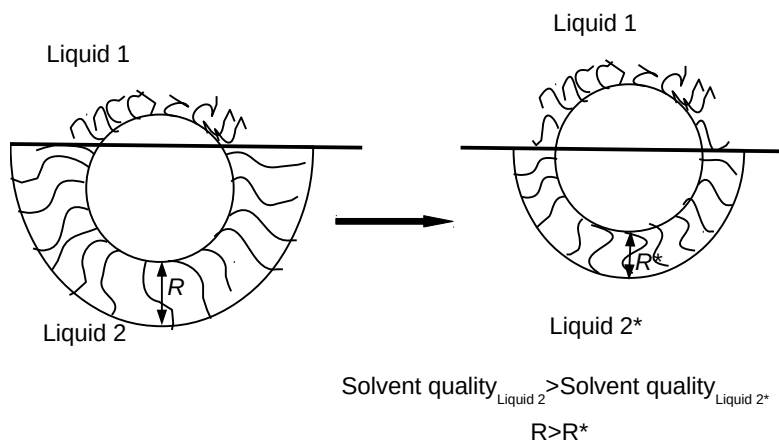


Figure 2.5: A schematic illustration of grafted polymers at a liquid-liquid interface, according to a model proposed by Isa et al. [75] before (left) and after (right) worsening the solvent quality of one of the solvents.

# Chapter 3

## Methods

### 3.1 Dynamic light scattering

In dynamic light scattering, the fluctuating intensity as a function of time is measured. The intensity at the detector,  $I(t)$ , fluctuates around an average value,  $\langle I(t) \rangle$ , due to the Brownian motion of the scatterers in the sample. The intensity autocorrelation function is given by [76]

$$g_2(q, \tau) = \frac{\langle I(t)I(\tau + t) \rangle}{\langle I(t) \rangle^2} \quad (3.1)$$

where  $\tau$  is the delay time. The angular brackets denote a time average. The magnitude of the scattering wave vector,  $q$ , is given by

$$q = \frac{4\pi n}{\lambda} \sin\left(\frac{\theta}{2}\right) \quad (3.2)$$

where  $n$  is the refractive index of the solvent,  $\lambda$  is the wavelength of the incident beam and  $\theta$  is the angle of the detected light with respect to the fully transmitted light (see figure 3.1). The field correlation function,  $g_1(q, \tau)$ , is the autocorrelation function of the electric field associated with the intensity and can for a monodisperse system be written as [77]

$$g_1(\tau) = e^{-D_c q^2 \tau} \quad (3.3)$$

provided the delay time is sufficiently short. Here  $D_c$  is the (collective) diffusion coefficient. The Siegert relation connects the field autocorrelation function and the intensity autocorrelation function according to [76],

$$g_1(q, \tau) = \sqrt{\frac{g_2(q, \tau) - 1}{\beta}} \quad (3.4)$$

where  $\beta$  is an instrumental factor that depends on the detection and is close to one for many light scattering setups based on single-mode fibers. The collective diffusion coefficient is for dilute systems equal to the single-particle self-diffusion coefficient,  $D$ . The hydrodynamic radius,  $R_h$ , can be calculated using

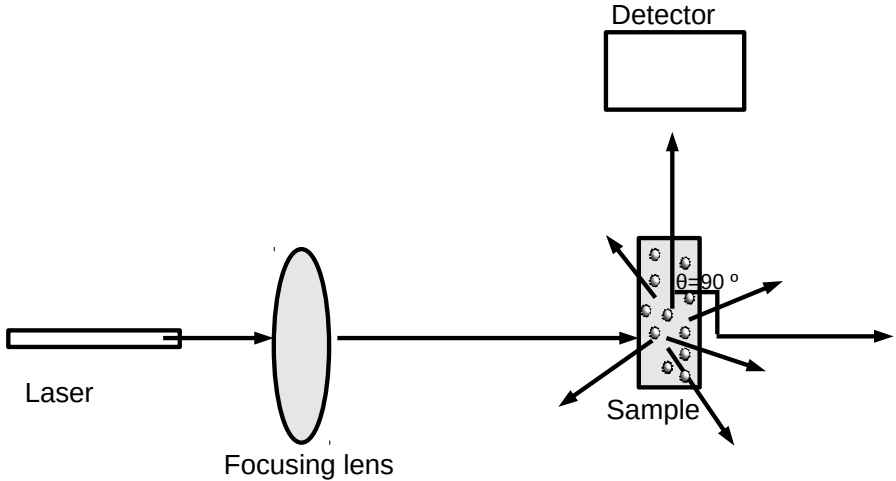


Figure 3.1: Schematic picture of the elements of a light scattering apparatus. The laser light source passes through a focusing lens and hits the sample. Some of the beam travels through the sample unaffected and some of the beam scatters. At an angle  $\theta$  compared to the unscattered beam, the scattered light is detected by a detector and is subsequently fed to a correlator for determination of the autocorrelation function.

the Stokes-Einstein equation

$$D_c \approx D = \frac{k_b T}{6\pi\eta R_h} \quad (3.5)$$

where  $k_b$  is Boltzmann's constant,  $\eta$  the viscosity of the solvent, and  $T$  is the temperature.

The DLS measurements in this work were performed using mainly an ALV CGS3 instrument with a He-Ne laser with a wavelength in vacuo of 632.8 nm. Also, a Malvern Zetasizer Nano ZS instrument was used, also equipped with a He-Ne laser. With the former instrument, the scattered light was detected at an angle of  $90^\circ$ , whereas  $173^\circ$  was used for the latter. The measurements were conducted at  $25^\circ\text{C}$ .

### 3.2 Small-angle scattering

In this work, both small-angle X-ray scattering (SAXS) and small-angle neutron scattering (SANS) have been used. In small-angle scattering (SAS), the intensity of the scattered beam is measured as a function of the scattering angle (see figure 3.2). One particularly simple case is for monodisperse spheres. In this case, the intensity,  $I(q)$ , can be written as a product of the so-called form

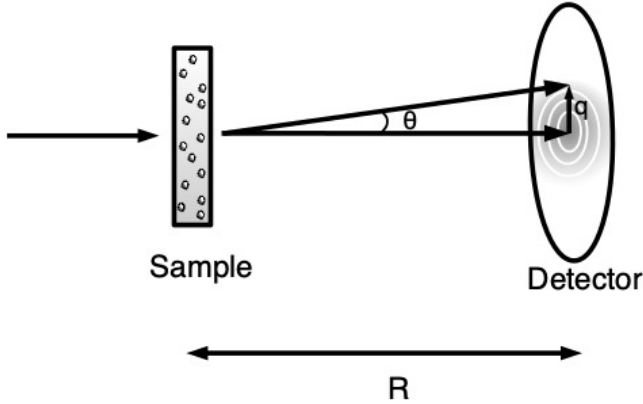


Figure 3.2: A schematic representation of an small-angle scattering experiment in transmission mode. The intensity is measured as a function of the scattering angle  $\theta$  using a position-sensitive detector placed at  $R$  meters from the sample to detect the small scattering angles. For small angles  $\sin \theta \approx \theta$  and then  $q$  is linearly related to the position on the detector.

factor,  $P(q)$ , and structure factor,  $S(q)$ :

$$I(q) = n_p P(q) S(q) \quad (3.6)$$

where  $n_p$  is the number density of the scatterers. The form factor depends on the shape and size of the particles and the structure factor appears because of interparticle correlations [78]. For dilute systems,  $S(q) = 1$  and the intensity then only depends on the form factor. For spherical particles,  $P(q)$  can be expressed as [62],

$$P(q) = (4\pi\Delta\rho)^2 \left( \frac{\sin qR - qR \cos qR}{q^3} \right)^2 \quad (3.7)$$

where  $R$  is the particle radius and  $\Delta\rho$  is the electron (SAXS) or scattering length (SANS) density difference between particle and solvent. It can be seen from equation 3.7 that the form factor will oscillate and that the minima of these oscillation will occur when  $\sin qR = qR \cos qR$ . Thus, the radius can be determined from the locations of the minima of the oscillations, the first of which occurs for  $qR \approx 4.5$ .

For a dilute polydisperse system,  $I(q)$  will depend on the scattering of each individual “size fraction”:

$$I(q) = \int n(R) P(R, q) dR \quad (3.8)$$

where  $n(R)$  is the number density of scatterers with a radius of  $R$  and  $P(R, q)$  is the corresponding form factor. The size distribution,  $n(R)$ , can be probed by

fitting the measured  $I(q)$  if some parametrized size distribution,, for instance a Gaussian one, is assumed for it.

Measurements have been carried out on two different SAXS instruments. One of the instruments, located at the Division of Physical Chemistry at Lund University, Sweden, is a laboratory-scale instrument using a wavelength  $\lambda = 0.154$  nm. The sample-to-detector distance was 1491.7 mm and the data were recorded using either a 2-pinhole or 3-pinhole collimation configuration and the SAXSGUI software was used in order to average the recorded data radially. The solvent was measured in the same capillary as the sample in order to subtract the background scattering. The scattering of water has also been measured in some cases to obtain the absolute intensity.

SAXS measurements were also performed at Beamline ID02 at the European Synchrotron Radiation Facility, ESRF, in Grenoble, France. All measurements were performed at room temperature at a wavelength of 0.995 Å or 1.381 Å. The samples were measured in a flow-through quartz capillary with an inner diameter of 1.95 mm or 1.6 mm. Several sample-to-detector distances were employed, 5, 10, 15 or 20 m. The time which the samples were exposed to the radiation varied between 0.01 s and 1 s depending on the particle concentration. In order to obtain the absolute intensity, and to correct for the background scattering, the scattering of water and solvent were measured separately in the same capillary as the sample.

The SANS measurements were carried out at the National Institute of Standards and Technology, NIST, in Gaithersburg, Maryland, USA. As for the SAXS experiments, all measurements were performed at room temperature and a neutron wavelength of  $\lambda = 6$  Å. For SANS the actual wavelength has a spread about this average of 10% using the particular set-up for the experiments reported here.

### 3.3 Cryo-electron microscopy

Cryo-electron microscopy, cryo-EM, is a type of transmission electron microscopy (TEM), where a thin sample is irradiated with an electron beam and the transmitted electrons are recorded. The main difference with conventional TEM is that the fluid sample is rapidly frozen in cryo-EM. The freezing has to be fast enough so that the fluid does not have time to crystallize. The vitrified sample is then placed in the microscope and illuminated with an electron beam. The electrons which are transmitted through the sample are recorded and a 2D picture is obtained [79, 80], as shown schematically in figure 3.3. If the freezing of the sample is done at high enough cooling rate the cryo-EM technique enables investigation of colloidal particles very close to their original state [81]. However, the particles are essentially confined to a monolayer.

In this work, all cryo-EM images were captured at the Department of Bioscience and Nutrition at Karolinska Institutet in Huddinge, Sweden. Glow-discharge holey carbon-coated copper grids were used and 3.5  $\mu\text{l}$  of the sample was applied in a controlled environment at 22 °C and a relative humidity close

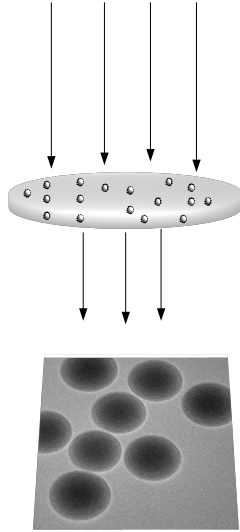


Figure 3.3: Schematic picture of the main idea of transmission electron microscopy. The electron beam is focused by electromagnetic lenses before hitting the thin sample. The transmitted electrons are first focused and then projected onto an image recording device and a 2D image is obtained [79].

to 100 %. After the samples were applied to the grid, excess sample was removed by blotting with filter paper which leaves a thin film. The samples were then rapidly frozen and then placed in the microscope which was operating at a 200 kV acceleration voltage. A CCD-camera was used in order to record the images.

### 3.4 Differential centrifugal photosedimentometry

In differential centrifugal photosedimentometry (DCP), a sample is exposed to a centrifugal force generated by the rotation of a disk containing a fluid medium. A light source illuminates the sample at the outer edge of the disk where a detector detects the change in light intensity as the particles pass. Since particles of different size scatter light disproportionately with respect to their size, the detected intensities are adjusted according to Mie theory [82, 83] to obtain the number size distribution.

For a spherical particle, the viscous drag arising from the fluid medium is, according to Stoke's law, written as [64]

$$F_d = -6\pi\eta Rv \quad (3.9)$$

where  $\eta$  is the fluid viscosity,  $R$  is the radius and  $v$  is the particle velocity.

### 3. METHODS

---

The viscous drag will slow the particle down. The driving force in DCP is the centrifugal force

$$F_s = \frac{4}{3}\pi R^3(\rho_p - \rho_0)\omega^2 r \quad (3.10)$$

where  $\rho_p$  and  $\rho_0$  are the densities of the particle and of the fluid, respectively,  $\omega$  is the angular velocity and  $r$  is the distance of the particle from the axis of rotation. When the forces balance, *i.e.* when  $F_d + F_s = 0$ , the steady state velocity,  $v_{ss}$ , can be expressed as

$$v_{ss} = \frac{2(\rho_p - \rho_0)R^2\omega^2 r}{9\eta} \quad (3.11)$$

From equation 3.11, it becomes clear that the velocities of particles exposed to a centrifugal force in a fluid are quite sensitive to their radii. This is valid assuming the particle dispersion is dilute enough so that no interactions between the particles are present.

Given that  $v_{ss} = \frac{dr}{dt}$ , equation 3.11 is in actuality a differential equation that relates particle position and time. Solving the equation, a relation between retention time,  $t$ , and particle radius [84, 82] is obtained as

$$R = \frac{1}{2} \left( \frac{18\eta \ln(r_d/r_i)}{\omega^2(\rho_p - \rho_0)t} \right)^{1/2} \quad (3.12)$$

where  $r_i$  and  $r_d$  are the radial positions initially and at the detector, respectively. In practice, however, a particle standard is used to calibrate the relation between retention time and particle size.

The measurements were carried out by first injecting a standard particle dispersion with known particle size, followed by the sample close to the center of the spinning disk. The spinning disk contained a gradient fluid, consisting in the present case of different concentrations of sucrose solutions. This method was mainly used as a complementary technique to SAXS in order to determine the size distribution and the polydispersity of different dispersions.

### 3.5 Pendant drop method

The shape of a liquid drop in another medium depends mainly on gravity and the surface tension between the two media. The surface tension manifests itself as a force that acts to minimize the surface area to make a spherical drop. Gravity pulls on the drop so it becomes oblong. The balance between these two forces gives a non-spherical drop. The shape of the drop, hanging on a needle, can be captured by a camera with illumination as illustrated in figure 3.4.

The surface tension of the pendant drop fulfills the Young-Laplace equation:

$$\gamma \left( \frac{1}{R_1} + \frac{1}{R_2} \right) = \Delta P = \Delta P_0 - \Delta\rho g z \quad (3.13)$$

Here,  $\gamma$  is the surface tension,  $R_1, R_2$  are the principal radii of curvature at the drop surface (these vary for non-spherical drops with the position on the

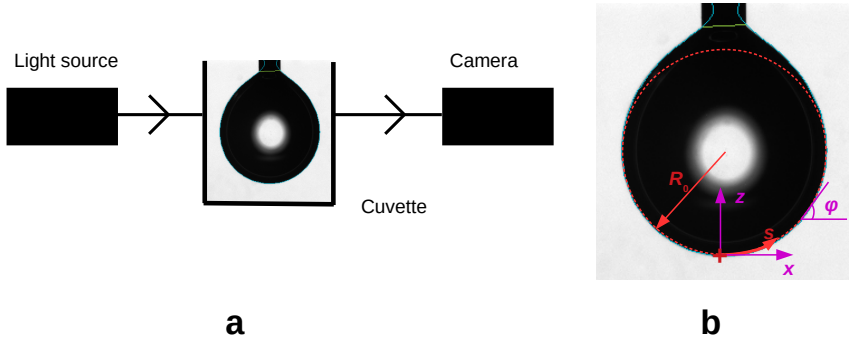


Figure 3.4: The main components of the experimental set-up for the pendant drop method are shown in panel a. A light source is used to illuminate a liquid drop, hanging from a needle (not to scale), a photo of which is recorded by a camera. The drop profile in the image is then fitted to a differential form of the Young-Laplace equation to obtain the surface tension. In panel b, the parameters and coordinate system used in the fitting of the differential Young-Laplace equation – which gives the surface tension – is shown. The blue line (hard to see in the figure) around the whole drop is the final fitting result using the green line at the top of the drop as a demarcation between the drop and needle.

surface),  $g$  is the gravitational constant,  $\Delta\rho$  is the density difference between the drop and the surrounding medium,  $z$  is the height above the apex of the drop, and  $\Delta P_0$  is the pressure difference at this point.

As seen in equation 3.13, the right-hand side depends only on a single coordinate,  $z$ . This means that there is symmetry around the  $z$ -axis. It can be shown [85] that equation 3.13 can be reformulated as the following three coupled differential equations

$$\begin{aligned}
 \frac{d\theta}{ds} &= 2 - \beta z - \frac{\sin \varphi}{x} \\
 \frac{dx}{ds} &= \cos \varphi \\
 \frac{dz}{ds} &= \sin \varphi
 \end{aligned}
 \tag{3.14}$$

Here,  $x$  is the horizontal coordinate of the drop surface,  $z$  is the corresponding one in the vertical direction,  $\varphi$  is the tangent angle and  $s$  is the distance from the apex along the drop surface, as seen in panel b in figure 3.4. All distances are normalized with respect to  $R_0$ , the spherical radius of curvature at

the drop apex. The parameter  $\beta$  is given by

$$\beta = \frac{\Delta\rho g R_0^2}{\gamma} \quad (3.15)$$

Solving the coupled differential equations in equation 3.14 yields in principle the functions  $x(s)$  and  $z(s)$  that describe the shape of the drop profile. This is done numerically for different values of  $\beta$  until the computed profile matches the experimental one (taking care not to include the needle's profile). The surface tension is then obtained through equation 3.15.

### 3.6 Synthesis and sample treatment

#### Chemicals and pre-treatment

In order to ensure the purity of the initiator, the potassium persulfate (KPS) was recrystallized prior to the synthesis. This was done by heating some water to about 60 °C and saturating it with KPS. The salt solution was then left in room temperature for several days to enable crystals slowly to form. The crystals were filtered and washed with water. Then, they were dried in an oven at about 40 °C.

The mPEGA2000 (SunBio, 99.8 %) with an average molecular weight (MW) of 2100 g/mol and mPEGA1000 (Alfa Aesar,  $\geq 95$  %, average MW = 1000 g/mol) were used as received. Styrene (Sigma Aldrich, 99.5 %), ethylene glycol dimethacrylate (EGDMA, Sigma Aldrich), mEGA130 (2-methoxyethyl acrylate, Sigma Aldrich, 98 %, average MW = 130 g/mol), mPEGA5000 (Sigma Aldrich, average MW = 5000 g/mol) and 2,2,3,3,4,4,4-heptafluorobutyl methacrylate (HFBMA, Alfa Aesar, 97%) contained either the polymerization inhibitor methyl ether hydroquinone (MEHQ) or hydroquinone (HQ) which both were removed prior to synthesis by passing the substance through a column packed with inhibitor removal resin (Alfa Aesar, CAS 9003-70-7). mPEGA 480 (Sigma Aldrich, average MW = 480 g/mol) contained both the inhibitors butylated hydroxytoluene (BHT) and MEHQ. In order to remove both inhibitors a column was packed both with the inhibitor removal resin previously used, and  $\text{Al}_2\text{O}_3$  (Fluka, purum p.a.).  $\text{Na}_2\text{SO}_4$  (99%, Sigma Aldrich) was heated to 450°C in an oven for 19 h prior to usage. All other chemicals were used as received.

#### Experimental set-up and execution

Two different synthesis set-ups have been used in this work: one smaller, employed in the group in the past [26], with some modifications made in this work, and a scale-up of this synthesis. The smaller original set-up will be explained first, followed by the scaled-up version.

In order to achieve monodisperse systems, different mPEGA:HFBMA molar ratios were used, depending on the molecular weight of the mPEGA (which will be discussed in Chapter 4). In a typical synthesis, the mPEGA was dissolved in 25 ml of Milli-Q (MQ) water and 11.6 mg of the initiator KPS is dissolved in



Figure 3.5: Synthesis set up for the 100 ml (left) and the 1000 ml (right) protocol.

10 ml of MQ water. The experimental set-up is shown to the left in figure 3.5. An Allihn condenser, a burette and an overhead stirrer were attached to a 250 ml three-necked round-bottom flask, immersed in an oil bath. The temperature of the oil bath was controlled by a hot plate and was kept at  $70^{\circ}\text{C}$ . In order to remove any dissolved oxygen, which can act as an inhibitor, 75 ml of MQ water was added to the round bottom flask and purged with  $\text{N}_2(\text{g})$ , for at least 30 minutes. The condenser was set to  $0^{\circ}\text{C}$  and was started the evening before in order to ensure that it reached its target temperature. The condenser was needed to prevent water and HFBMA (boiling point around  $134\text{-}136^{\circ}\text{C}$ ) from evaporating. In order to make the cooling of the condenser more efficient, the round-bottom flask was immersed no further than to the total volume of liquid that was to be added. The overhead stirrer was used with a polypropylene stirring rod and blade employing a stirrer bearing to prevent evaporation from the flask neck holding the stirring rod.

When the MQ water has been purged with  $\text{N}_2(\text{g})$  for at least 30 minutes, the stirring rate was set to 500 rpm and the mPEGA solution was added rapidly followed by 1 ml of HFBMA. The stirring was continued for one hour and was then decreased to 150 rpm. After the stirring rate was decreased, the KPS solution was added dropwise, using a burette, during 1.5-2 hours. To avoid  $\text{O}_2(\text{g})$  entering the system, a gentle flow of  $\text{N}_2(\text{g})$  was maintained at the top of the burette and the condenser. After all of the initiator was added, the system was closed and the gas was turned off. The synthesis was then left overnight.

The day after, the heat was turned off and the dispersion is left to slowly cool.

When increasing the synthesis volume by a factor of 10, going from 100 ml to 1000 ml, some changes had to be made. A 2 l, four-neck round-bottom flask was used instead of the 250 ml three-neck one. This was done not only due the greater reaction volume, but also to improve cooling and a second condenser was connected to the additional neck. Previously [26], both the rate of addition of the initiator solution and the stirring rate were shown to be important for monodispersity and yield. However, in a scale-up of the synthesis, it is neither clear how to scale the addition rate of the initiator solution, nor its concentration volume to be added. In a first attempt, the stirring rate was kept the same as in the 100 ml protocol – but the stirring blades were approximately twice as long – and the concentration of the initiator was 10 times as high in a volume that was 2.5 times as large. The mPEGA was treated in a similar manner: the amount was a factor 10 larger, dissolved in MQ-water to a total volume of 50 ml – twice the volume in the smaller-scale protocol. In addition, to make the addition of the initiator consistent, a syringe infusion pump was used and the addition speed was set to 12 ml/h so that the total addition time was the same as for the smaller-scale protocol. Using this approach resulted in a yield and polydispersity comparable to that of the 100 ml synthesis.

#### Post-treatment of dispersions

The purification of unreacted reagents was done differently depending on the size of the batch. In both cases, the dispersion was first filtered through a Munktell(R) filter paper (grade 00R, size 10  $\mu\text{m}$  or grade 1001, size 2-3  $\mu\text{m}$ ) using a Büchner funnel under atmospheric pressure. For the smaller (100 ml) semi-batch synthesis, the dispersion was then dialyzed against deionized water, using dialysis tubes with a cut-off MW of 300 kDa (Spectra/Por) or 12-14 kDa (MAKAB) depending on the mPEGA MW. The water was changed periodically. The conductivity of the dialysis water was monitored in order to determine when the KPS concentration had diminished, and, when the water was changed, the amount of foam caused by the mPEGA was checked. When there was no increase in the conductivity and no foam was seen, the dialysis was considered complete. Normally, this took between 5 and 7 days.

After the dialysis, NaCl and  $\text{NaN}_3$  were added to the dispersion, resulting in a total salt concentration of 10 mM (7 mM and 3 mM, respectively). This was done to improve the long-term storage of the dispersion. The  $\text{NaN}_3$  prevents bacterial growth [86] and contributes, along with the NaCl, to the screening of any potential electrostatic interactions between the particles.

For the 1000 ml protocol, another type of purification scheme was needed due to the large dispersion volume. A cross-flow dialysis system (Vivaflow<sup>TM</sup> 200, Sartorius) with a 50 kDa molecular weight cut-off (MWCO) polyethersulfone membrane was used instead of the dialysis tube. At first, the dispersion was dialyzed against MQ-water until the conductivity was equal to that of pure water. Subsequently, the concentration of the dispersion was increased by a factor of two by stopping the refilling of MQ-water. In order to introduce

the background salt (7 mM NaCl and 3 mM NaN<sub>3</sub>), the dispersion was dialyzed against the background salt solution until the conductivity of the “spent” dialysate matched that of the “fresh” dialysate.

After the synthesis, the concentration of particles in the dispersion was often rather low, typically around 0.15-1 % (depending on the MW of the mPEGA used and molar ratio of mPEGA to HFBMA). For SAXS measurements, cryo-EM imaging and some of the DLS measurements higher particle concentrations were needed. In order to increase the particle concentration, the dispersion was centrifuged. To avoid too high centrifugal forces, which could damage the particles, a Jumbosep<sup>TM</sup> centrifugal device (Pall Inc.) with a 30 kDa MWCO membrane was used. Additionally, the same device was used when changing the solvent. First, the dispersion was concentrated and then the dispersion was diluted with the desired solvent and then recentrifuged. When the filtrate had the same density as the exchange solvent, the solvent exchange was deemed complete. This procedure was employed to exchange water for D<sub>2</sub>O in samples for SANS measurements.

### 3.7 Scattering models with structure factor

Even though great care has been taken to synthesize particles which are monodisperse as possible, there still exists some polydispersity moreover, in some cases, the size distributions have been found to be non-symmetrical with a “tail”-like appearance extending to smaller particle sizes. In order to account for this asymmetry, the size distribution in equation 3.8 is modeled as the sum of two Gaussian distributions

$$n(R) = x_1 n_1(R; \bar{R}_1, \sigma_1) + x_2 n_2(R; \bar{R}_2, \sigma_2) \quad (3.16)$$

where  $x_1$  and  $x_2$  are mole fractions and add up to unity, and  $n_1$  and  $n_2$  are Gaussian distributions with mean values  $\bar{R}_1$  and  $\bar{R}_2$  and standard deviations  $\sigma_1$  and  $\sigma_2$ , respectively. The superposition of these two distributions allow for modeling skewed overall distributions.

In many cases when modeling the scattering intensity, it is enough to use only the form factor. However, when solvent conditions become poor, particles begin to interact even under dilute conditions. In these cases, the structure factor also has to be implemented in the scattering model. Consider the scattering from many particles with form factor amplitudes  $F_i(q)$ :

$$I(q) = \frac{1}{V} \left\langle \sum_{i=1}^N \sum_{j=1}^N F_i(q) F_j(q) e^{i\vec{q} \cdot \vec{r}_{ij}} \right\rangle \quad (3.17)$$

If it is assumed that there is no correlation between particle size and relative position, a common form factor can be computed from the form factor amplitudes as the weighted average over the particle size distribution to yield

$$I(q) = \frac{1}{V} \sum_{i=1}^N \sum_{j=1}^N \langle F_i(q) F_j(q) \rangle \langle e^{i\vec{q} \cdot \vec{r}_{ij}} \rangle \quad (3.18)$$

### 3. METHODS

---

Where the last average is an ensemble average. The first average is over all pairs of particles and may be rewritten in terms of averages over all single particles [87]

$$\langle F_i(q)F_j(q) \rangle = [\langle F(q)^2 \rangle - \langle F(q) \rangle^2] \delta_{ij} + \langle F(q) \rangle^2 \quad (3.19)$$

In all, this is the so-called ‘‘decoupling approximation’’. Inserting eq. 3.19 into eq. 3.18, yields

$$I(q) = nP(q)S_{\text{eff}}(q) \quad (3.20)$$

$$S_{\text{eff}}(q) = 1 + \beta(q)[S(q) - 1] \quad (3.21)$$

$$\beta(q) = |\langle F(q) \rangle|^2 / \langle F(q)^2 \rangle \quad (3.22)$$

where

$$S(q) = \frac{1}{N} \left\langle \sum_{i,j}^N e^{i\vec{q} \cdot \vec{r}_{ij}} \right\rangle \quad (3.23)$$

is the structure factor of a monodisperse system.

The above approximations fail to model the strong upturn at low  $q$ , and the significant suppression at somewhat higher  $q$ , that arise from the colloidal particles forming clusters upon large-enough salt additions. The scattering from the clusters can be modeled with an additional term of Debye-Bueche form [88, 89, 90] in the effective structure factor in equation 3.21. The effective structure factor is then written as

$$S_{\text{eff}}(q) = 1 + \beta(q)[S(q) - 1] + \Delta S(q) \quad (3.24)$$

where the  $\Delta S(q)$  is

$$\Delta S(q) = \frac{C}{(1 + (q\xi)^2)^2} \quad (3.25)$$

Here,  $C$  is proportional to the average mass and  $\xi$  to the size of the particle clusters.

# Chapter 4

## Results

The following results are based largely on Papers I - IV, which are appended to this thesis.

### 4.1 Paper I

In Paper I, the versatility of the synthesis procedure, which was developed earlier in the group [26], is investigated. Different lengths of the mPEGA polymer, 480 g/mol, 5000 g/mol and 2000 g/mol (same as in Ref. [26]), have been used in order to obtain different thicknesses of the grafted layer (however, no results for the 480 g/mol polymer will be discussed here). Further variations of the synthesis were undertaken in this paper, such as crosslinking of the particles and replacing the HFBMA of the core with polystyrene. Some adjustments had to be made to the mPEGA:monomer molar ratio for the different syntheses in order to keep the polydispersity low.

Two different batches with the HFBMA cores replaced with polystyrene were synthesized. The hydrodynamic radii of the two batches were measured by DLS. The results of SAXS measurements were interpreted qualitatively, without model fitting, to get an idea of the polydispersity. In the one synthesis, the initiator was added all at once (a batch synthesis), while in the other, the previously described semi-batch protocol was used. The SAXS data (not shown) from the dispersions obtained from the semi-batch synthesis exhibit more resolved form factor minima and it was therefore concluded that this batch was less polydisperse.

Four of the syntheses were performed with the mPEGA5000 with different mPEGA:HFBMA molar ratios. The size of the particles varied with the different molar ratios, with the syntheses with the highest molar ratios yielding the smallest particles and vice versa. The DCP measurements revealed that, compared to the synthesis using mPEGA2000 polymer in Ref. [26], a lower molar ratio was needed in order to obtain monodisperse particles. Furthermore, one of the batches had two peaks in the size distribution and was excluded from further studies.

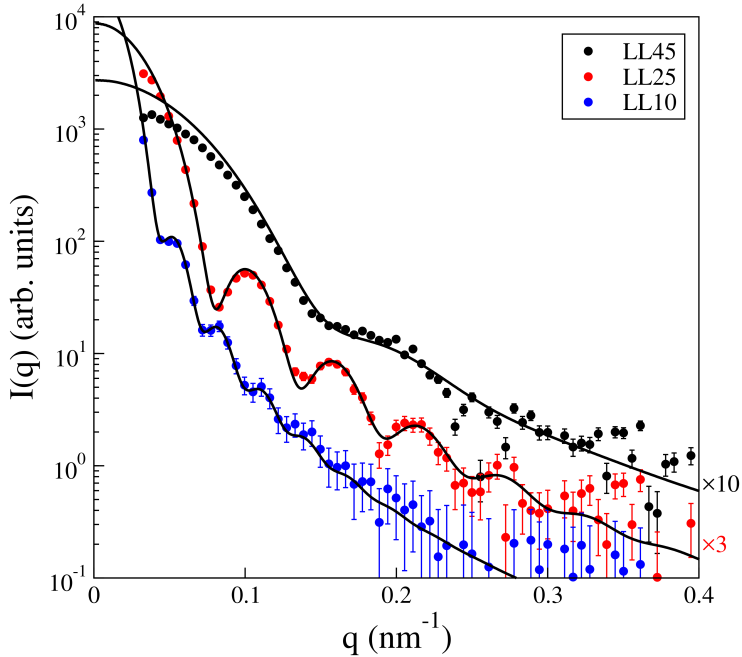


Figure 4.1: SAXS data of three of the batches obtained using mPEGA5000. Some of the intensities have been scaled by the factors given on the right of the figure, for clarity. The LL45 batch has a molar ratio mPEGA:HBMA of 0.045, the LL25 batch has one of 0.025 and the LL10 batch has one of 0.01. The solid lines are form factor fittings according to equation 3.8.

In-house SAXS measurements, on dilute dispersions, were performed on three of the mPEGA5000 batches and fitted to equation 3.8, assuming form factors of homogeneous spheres for all sizes of the distribution needed to capture the polydispersity. The size distribution was modeled as a superposition of two Gaussian distributions, each defined by a mean radius and a standard deviation. As seen in figure 4.1, the mean radii of the different batches differ as seen from the positions of the form factor minima shifting along the  $q$ -axis. This is also evident from the DCP measurements (not shown). The fitting works well for the batches with the larger particles but not for LL45 which contains the smallest particles. This might be due to the increased relative layer thickness. The mPEGA layer is assumed to not contribute to the overall scattering due to the high scattering contrast of HFBMA. This assumption might not hold for the LL45 batch where there is relatively less HFBMA.

In figure 4.2, cryo-EM images of the particles grafted with mPEGA5000 are shown. The mPEGA layer can be seen as a “halo” around the particles and it can also be seen that the particles are not in direct contact with each other, presumably because the polymer grafts prevent this. The mean particle size

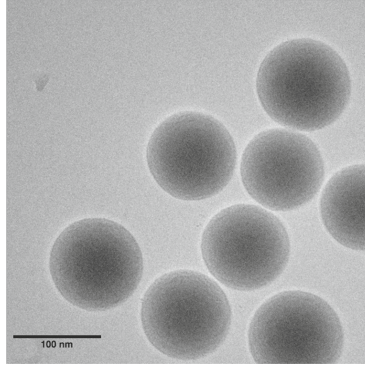


Figure 4.2: Cryo-EM image of particles grafted with mPEGA5000 (the LL25 batch).

obtained from the cryo-EM images is about 10 % smaller than the one obtained from the SAXS form factor fitting. This might again be due to the mPEGA layer contributing more than expected to the scattering in SAXS, resulting in an apparent larger core size. The stability of the different batches was tested against  $\text{Na}_2\text{CO}_3$  addition. The two batches with the lowest molar ratios became unstable at lower salt concentrations. This suggests that these two batches had a lower mPEGA coverage.

The synthesis protocol for particles grafted with mPEGA5000 polymers was further developed in order to produce crosslinked particles. This was done so that non-aqueous media, such as methanol and ethanol, could be used without uncontrolled swelling of the particles. The mPEGA:HFBMA molar ratio was kept at 0.025, since that yielded monodisperse particles with sufficient stability against salt addition. The monomer EGDMA was used as crosslinker and three different EGDMA:HFBMA molar ratios were evaluated. Whether or not the crosslinking was successful was determined by DLS measurements of the dispersions in tetrahydrofuran (THF). The non-crosslinked LL25 batch was used as a reference and these particles showed uncontrolled swelling when transferred to THF. The crosslinked particles, however, showed significantly less swelling, with less swelling the higher the EGDMA:HFBMA molar ratio.

## 4.2 Paper II

The versatility of the synthesis was extended in Paper II where additional particles with different grafting layer thicknesses, compared to Paper I, have been synthesized. Since the core of the particles has a refractive index close to that of water, leading to a weak core-core vdW attractions, the effect of the interactions between the polymers can be studied in solution. For this purpose, having different shell thicknesses becomes valuable.

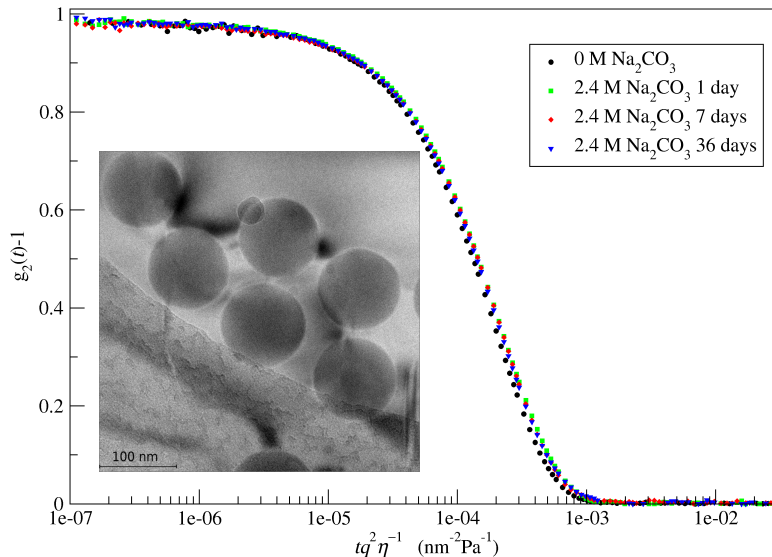


Figure 4.3: DLS measurements of particles grafted with mEGA130 in 0 M  $\text{Na}_2\text{CO}_3$  and in 2.4 M  $\text{Na}_2\text{CO}_3$  after several days. No change is observed, indicating stability. Inset: Cryo-EM image of particles grafted with mEGA130 with a mEGA:HFBMA molar ratio of 0.05 in 0 M  $\text{Na}_2\text{CO}_3$ .

Here, mPEGA1000 and single ethylene glycol (mEGA130) grafts were employed to yield two new shell thicknesses. The particles grafted with mEGA130, resulting in a molecular shell thickness, can be seen in the inset of figure 4.3. Several syntheses with different mEGA:HFBMA molar ratios were performed and a molar ratio of 0.05 was concluded to be the best; this was the highest molar ratio that did not result in a significant polydispersity. As for the particles grafted with mPEGA1000, several syntheses were performed. Figure 4.4 shows cryo-EM images for the batch of grafted particles with mPEGA1000 with a molar ratio, mPEGA:HFBMA, of 0.08. As can be seen in the image, this molar ratio yielded a bidisperse system. Even if both size fractions by themselves seem monodisperse, this type of polydispersity is not ideal.

The stability when adding  $\text{Na}_2\text{CO}_3$  to the dispersions was investigated. The particles with the shortest grafts (mEGA130) proved to be exceedingly stable, both over long and short term. In fact, these could not be destabilized at all using  $\text{Na}_2\text{CO}_3$  at room temperature. Figure 4.3 shows DLS measurements for these particles, which were performed in 2.4 M  $\text{Na}_2\text{CO}_3$ . It is clear that

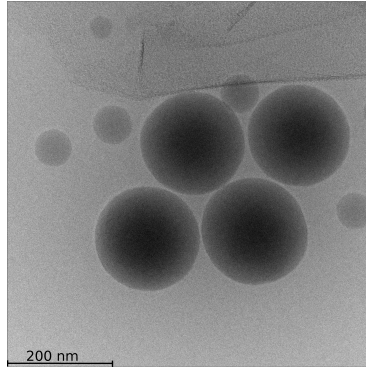


Figure 4.4: Cryo-EM image of particles grafted with mPEGA1000. The molar ratio mPEGA:HFBMA was 0.08, and as can be seen, this molar ratio did not yield a completely satisfactory monodispersity.

the form of the autocorrelation function remains unchanged even after several weeks. Moreover, it is close to the autocorrelation function recorded for the same particles in the absence of  $\text{Na}_2\text{CO}_3$ , when the change in viscosity and refractive index due to  $\text{Na}_2\text{CO}_3$  is accounted for. In figure 4.3 this has been done by scaling the delay time with the relaxation time  $(q^2 D_0)^{-1} \sim \eta/q^2$ .

In past work [91] it was noted that particles grafted with mPEGA2000 became unstable at the same  $\text{Na}_2\text{CO}_3$  concentration regardless of the particle concentration. To examine whether or not there is a particle concentration dependence of the stability upon salt addition for these PEG-grafted particles, SAXS measurements were performed at the ESRF. For this purpose, two different particle concentrations of particles grafted with mPEGA1000 polymers with a mPEGA:HFBMA molar ratio of 0.05 were transferred to solutions of varying  $\text{Na}_2\text{CO}_3$  concentrations. The results are shown as measured intensities as a function of  $q$  in figure 4.5. The dispersions are observed to be stable up to 0.5 M of salt. At higher salt concentrations, the intensity is increased in the low  $q$ -range which indicates that aggregates are present, which is interpreted as an instability. Regardless of the particle concentration, the stability behavior of the dispersion with  $\phi \approx 1.2\%$ , upper set, is nearly quantitatively the same as the behavior of the lower set, for which  $\phi$  is about ten times lower.

The reason for the lack of effect of the particle concentration on the stability limit is unexpected. Forming aggregates is the result of changes in both entropy (which opposes it since the local particle concentration increases) and energy (which must favor it if it is to occur in this case) and the entropy change should be concentration dependent (as for a gas). At lower concentrations, the entropy should oppose aggregate formation more strongly. If the stability limit remains the same, it would imply stronger attractions. However, why would the attractions become stronger at lower concentrations? Another explanation is needed.

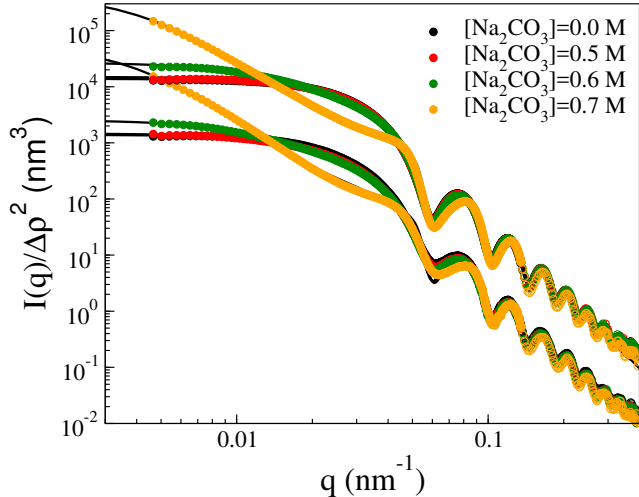


Figure 4.5: SAXS measurements of particles grafted with mPEGA1000 polymers. Different amounts of  $\text{Na}_2\text{CO}_3$  have been added to the dispersions. The two measurements series, upper and lower, have two different particle concentrations. The upper has a volume concentration of  $\sim 1.2\%$  and the lower one of  $\sim 0.1\%$ . The stability of the dispersions is independent of the particle concentration: both dispersions are stable at salt concentrations up to and including 0.5 M. The increase in intensities in the lower  $q$ -range, at 0.6 M and 0.7 M of  $\text{Na}_2\text{CO}_3$ , indicates instability. All intensities have been scaled by the excess scattering contrast. The solid lines are model fits.

Salt-induced dewetting of the PEG-shell would favor particle clustering because of changes in the entropy of the PEG-shell and hydration water. This entropy change (per particle) would be independent of the particle concentration, i.e. a single-particle effect. The salt concentration needed to bring about this proposed dewetting would also be independent of particle concentration. In this model, it is not long-range particle-particle attractions such as electrostatic or van der Waals forces that cause the aggregates to form.

The data in figure 4.5 are fitted to a scattering model. The measurements performed at 0 M and 0.5 M  $\text{Na}_2\text{CO}_3$ , can be fitted to equations 3.7 and 3.8, modeling the size distribution as the sum of two Gaussian distributions. The increase at the two higher concentrations, 0.6 M and 0.7 M, requires a structure factor in the model. The structure factor  $S(Q)$  was modeled with an attractive hard-core Yukawa potential,

$$\frac{u(r)}{k_B T} = \begin{cases} \infty, & r \leq d \\ -\frac{K e^{-b(r/d-1)}}{r/d}, & r > d \end{cases} \quad (4.1)$$

where  $k_B T$  is the thermal energy,  $r$  is the separation between particles,  $d$  is the

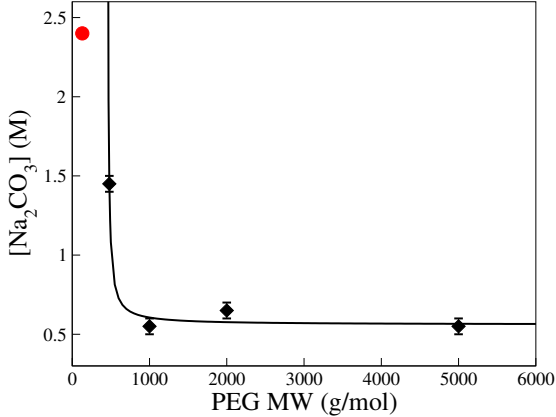


Figure 4.6: The stability limit of particles grafted with mPEGA of different MW, in terms of added  $\text{Na}_2\text{CO}_3$ . The red circle represents the highest salt concentration that was possible to obtain, and even at this concentration the particles grafted with mEGA130 were still stable. The solid line is a fit using equation 4.5 with the fitting parameters  $m = 7.44$  (429 g/mol) and  $k_{\text{EG}} = \chi^*/(0.56\text{M})$ .

hard-core diameter,  $b$  is a range parameter and  $K$  is the contact value of the potential. In this work,  $b$  was set to 100, modeling the width of the potential as very narrow. A monodisperse  $S(q)$  was used, neglecting the correlations between sphere size and position in employing the decoupling approximation [87]. The mean-spherical approximation theory [92, 93] was used to yield semi-analytical solutions for  $S(q)$ . For the 0.7 M data, the extra term of Debye-Bueche form, in equation 3.23, was used in order to model the large upturn at low  $q$  and the suppression at intermediate  $q$ .

The stability limit, in terms of added  $\text{Na}_2\text{CO}_3$ , of particles grafted with different mPEGA MW is shown in figure 4.6. The stability limit is fairly constant until a MW of 1000 g/mol. For grafted mPEGA polymers shorter than that, the stability is higher. The red circle represents particles grafted with mEGA130, which could not be destabilized. The solid line in figure 4.6 is a curve resulting from fitting to a Flory-Huggins parameter-based theory. The Flory-Huggins parameter,  $\chi$ , of the polymer has contributions both from the repeating part of the mPEGA chain, ethylene glycol ( $\chi_{\text{EG}}$ ), and from the non-repeating terminal ends of it, the methoxy group ( $\chi_{\text{rest}}$ ). The Flory-Huggins parameter is assumed to be an average of these contributions,

$$\chi = \frac{n\chi_{\text{EG}} + \chi_{\text{rest}}}{n + 1} \quad (4.2)$$

where  $n$  is the number of ethylene glycol units. The grafted polymers on the particles are assumed to have a brush configuration. This gives rise to geometrical constraints where the solvent is prevented from reaching the inner ethylene

glycol groups as found in computer simulations [94]. Correcting for this in the average, the  $\chi$  parameter can be expressed as

$$\chi = \frac{(n-m)n\chi_{EG} + \chi_{rest}}{n-m+1} \quad (4.3)$$

where  $m$  is the number of inaccessible units (with  $m < n$ ). Assuming that the  $\chi_{EG}$  parameter has a linear dependence on the salt concentration,  $C$ , with a constant of proportionality  $k_{EG}$ , we can write

$$\chi_{EG} = k_{EG}C \quad (4.4)$$

meaning that pure water is assumed to be close to, but slightly better than, a  $\theta$  solvent for the polymer. Assuming that adding salt will lead to  $\chi$  becoming at some point large enough to destabilize the particles, which requires that  $k_{EG} > 0$ . If  $\chi = \chi^*$  when the particles become unstable at the concentration  $C^*$ , taken to correspond to the salt concentrations in figure 4.6, we obtain

$$C^* = \left( \chi^* - \frac{1}{n-m+1}\chi_{rest} \right) \frac{n-m+1}{(n-m)k_{EG}} \quad (4.5)$$

In the fit in figure 4.6, equation 4.5 was used and  $\chi_{rest}$  was set arbitrarily to zero and  $\chi^*$  was set to  $1/2$ , thereby setting solvent conditions at the point of instability to  $\theta$  conditions. This leaves only  $m$  and  $k_{EG}$  as fitting parameters. This model stresses that it is the unfavorable interaction between salt-containing solvent and the polymer graft that causes particles to cluster.

### 4.3 Paper III

In this Paper, further efforts have been made to investigate the salting out of PEG chains grafted on colloidal particles. In this case, mPEGA2000-grafted particles have been used. Both the stability, employing SANS, and the interfacial activity, investigated by the pendant drop method, are studied as the solvent quality is worsened by adding salt. As mentioned earlier in the Background, PEG has been shown to be both surface and interfacial active. It should then follow that particles covered by a PEG-layer may exhibit similar properties as free PEG. Furthermore, in the interfacial activity studies, the particles have an opportunity to escape the worsened aqueous solvent by moving to the interface or even the oil phase. Indeed, nanoparticles grafted with PEG have been found to be surface active [95, 96, 97, 98, 22, 23, 21, 24]. It has also been shown, via computer simulations, that the grafted polymers on nanoparticles at liquid-liquid and liquid-air interfaces deform [99, 100]. However, the particles used in this work are far larger than the typical nanoparticles, resulting in the PEG-shell being relatively smaller in size compared to the whole particle. This might have a significant effect on the behaviour, at least for particles with densely grafted brushes that presumably are more constrained and cannot deform as much as sparsely grafted chains.

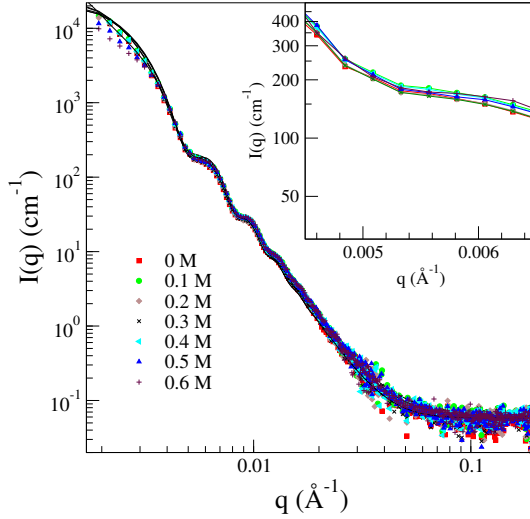


Figure 4.7: The scattering intensity  $I(q)$  as a function of the magnitude of the scattering vector  $q$  for particles grafted with mPEGA2000 (1 wt%), dispersed in  $\text{D}_2\text{O}$  at different concentrations of  $\text{Na}_2\text{CO}_3$ , as labeled. The solid lines are form factor fits, aside from the 0.5 M case which includes a structure factor. A decrease in the intensity at small  $q$  can be seen for the higher concentrations. The inset shows a close-up of the first form-factor “minimum” practically no difference depending on the salt concentration can be seen (the solid lines are here guides to the eye).

In order to achieve more concentrated dispersions needed in the SANS studies, a scale-up of the original synthesis was undertaken, as described in the Background. However, as the particle concentration of the stock dispersion increased, it became difficult to mix samples with precise particle concentrations. This was due to the highly concentrated stock dispersion not being completely homogeneous. This is noticeable in figure 4.8 where the data had to be vertically shifted to overlap the points with for data without any  $\text{Na}_2\text{CO}_3$ .

Typically,  $\text{D}_2\text{O}$  is used in neutron scattering experiments instead of  $\text{H}_2\text{O}$  due to its lower incoherent scattering or to selectively vary the contrast in order to study aspects of microstructure [101]. For this reason, measurements on the mPEGA2000-grafted particles were conducted in  $\text{D}_2\text{O}$  and different concentrations of  $\text{Na}_2\text{CO}_3$ , with the results shown in figure 4.7. The different measurement series overlap that of the data at 0 M up until the two highest salt concentrations. The ones below 0.5 M have been fitted to a core-shell form factor. At higher concentrations, a decrease in the intensity at low  $q$  can be seen which is due to interparticle interactions causing cluster formation. In order to capture this, a structure factor was calculated for a Yukawa potential, complemented with the decoupling approximation and MSA theory as in Paper

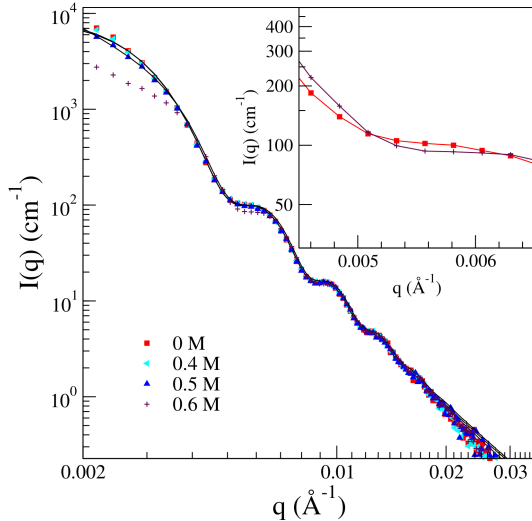


Figure 4.8: SANS measurements of particles grafted with mPEGA2000 (15 wt.%) dispersed in a 0.5 v/v D<sub>2</sub>O/H<sub>2</sub>O mixture. Here,  $I(q)$  is shown as a function of  $q$ . The data have been fitted to a form factor and additionally to a structure factor at 0.5 M; the fittings are shown as the solid lines. The inset shows a shift to higher  $q$  at the first minima for 0.6 M (the solid lines are here guides for the eye).

II. It can be seen in the inset of figure 4.7 that there is essentially no difference in the first form factor “minimum” at the different salt concentrations.

Furthermore, mixing D<sub>2</sub>O and H<sub>2</sub>O changes the contrast so that certain features can be enhanced. In this case the contrast of PEG grafts can be improved to examine whether any changes occur as the particles begin to aggregate. However, precaution must be taken when exchanging some of the H<sub>2</sub>O for D<sub>2</sub>O since the solubility, and thereby also the interactions, of PEG changes in D<sub>2</sub>O [102, 103]. The ratio H<sub>2</sub>O:D<sub>2</sub>O of 2:1 was chosen so that changes in the PEG-layer become more readily observable in the scattering signal. The results can be seen in figure 4.8. The form factor alone can be used to fit the results for the 0 M and 0.4 M measurements but, just as in the D<sub>2</sub>O case, there is a decrease in  $I(q)$  for low  $q$  at 0.5 M and 0.6 M. The structure factor from MSA theory can be used in the 0.5 M case, but it fails to capture the more pronounced decrease at 0.6 M. To model this case, a cluster contribution has to be added to the theory [104, 88, 89].

Contrary to the measurements performed in pure D<sub>2</sub>O, the first “minimum” in figure 4.8, as seen in the inset, is shifted to higher  $q$  for the 0.6 M Na<sub>2</sub>CO<sub>3</sub> case. The shift can be modeled by decreasing the shell thickness by 5 Å and decreasing the shell SLD. This suggests that the shell becomes dehydrated: the decrease in SLD corresponds to less H<sub>2</sub>O/D<sub>2</sub>O being present in the shell. A

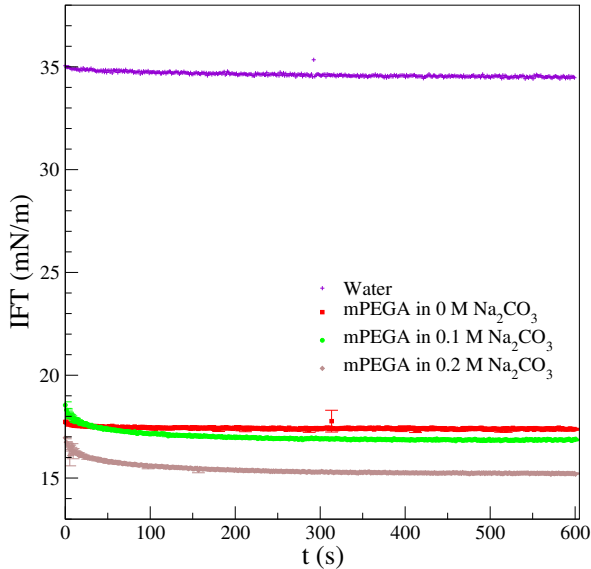


Figure 4.9: The interfacial tension between toluene and mPEGA(aq) progressing in time for varying concentrations of  $\text{Na}_2\text{CO}_3$ .

decrease in the shell thickness has been determined in earlier work for the same type of particles in cryo-TEM measurements [91].

PEG is both soluble in water and toluene [105]. If the PEG-layer is dewetted when adding a salting-out salt, the PEG-covered particles might either migrate to the toluene-water interface or to the toluene bulk phase. To examine this partitioning in a qualitative manner, Pickering emulsions were produced by sonicating toluene with dispersions containing mPEGA-grafted particles both in the presence of sodium carbonate salt and without it. The emulsions are stable for a period of weeks in both cases. However, in the case where no salt was added, the emulsion layer was thinner and particles were not only present in the emulsion but also in the aqueous phase below. It is a clear indication that the particles avoid the aqueous bulk phase when salt is added.

This migration to the oil-water interface can be captured more quantitatively by measuring the interfacial tension between the toluene and the dispersion phases. First, however, the pendant drop method was used to measure the IFT between aqueous solutions containing 0.1 wt.% free mPEGA and varying concentrations of  $\text{Na}_2\text{CO}_3$ . The results are shown in figure 4.9. As seen, mPEGA is clearly surface active, lowering the IFT by more than a factor of ten, compared to the pure water and toluene value of 35 mN/m, even when no salt is added. The IFT is even further lowered as salt is introduced.

Initial IFT measurements on the grafted particles, with and without salt (not shown here), did also show a decrease in the IFT. However, care has to be

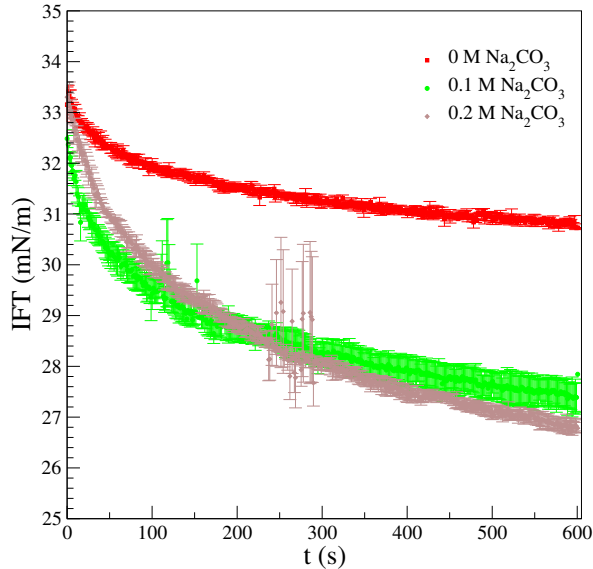


Figure 4.10: Interfacial tension as a function of time for mPEGA2000-grafted particles in different concentrations of salt, as labeled. The particle concentration was 0.2 wt.% and a hook-needle was employed in order to have the dispersion as the surrounding medium instead of the toluene. The IFT decreases as salt is added.

taken when doing these measurements since clusters are formed when enough salt is added. These clusters sediment to the bottom of the dispersion drop. This leads to an apparent larger IFT since  $\Delta\rho$  in equation 3.15 becomes larger when the particles sediment. In order to avoid this problem, a hook-needle was employed which enables the lighter phase (toluene) to be the drop and the heavier phase (dispersion and salt) to be the surrounding medium. However, a lower concentration of particles had to be used in order for the drop to be visible. Since the IFT is sensitive to even small amounts of impurities, the particles were additionally dialyzed using dialysis tubes to remove any unreacted PEG that had not been removed during a previous cross-flow dialysis step.

In the experiments the effect on the IFT of adding particles, seen in figure 4.10, was less dramatic compared to free mPEGA. This finding is likely caused by the PEG being confined to the particle surfaces. A lower decrease of the surface tension was for instance observed by Raffa et al [106] for PEGA polymerized into a comb structure compared to free PEGA monomer. Nevertheless, as is clear from figure 4.10, in which the particle concentration was kept constant, the IFT is lowered more with increasing salt concentration, which supports the hypothesis of a salt-induced dehydration of the PEG-layer as the driving force. Moreover, the results obtained here show that also larger colloidal par-

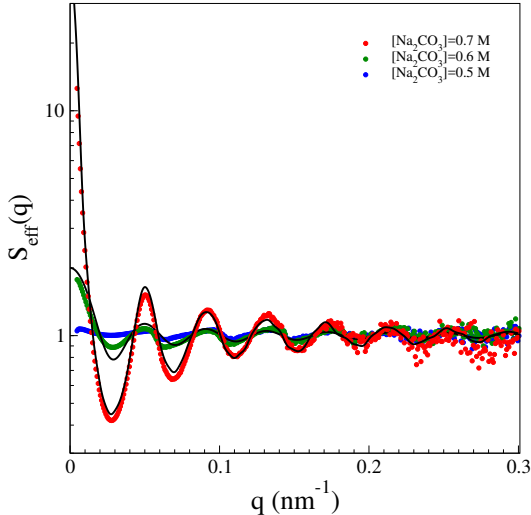


Figure 4.11: The effective structure factor plotted against  $q$  for particles grafted with mPEGA1000. The data is taken from figure 4.5 for  $\phi \sim 0.012$ . The solid lines are fittings using a 2-cluster or 40-cluster model, respectively.

ticles are driven to the interface through salting-out and not just nanoparticles [21, 22, 23, 24].

#### 4.4 Paper IV

As has been demonstrated in Paper II, the aggregation of the particles is independent of particle concentration. It was also noted that conventional liquid state theory cannot model the low- $q$  behavior at high salt concentrations, specifically the large upturn. Also the high- $q$  behavior is affected, as seen in the effective structure factor, defined as  $S_{\text{eff}}(q) = I(q)/(nP(q))$ , in figure 4.11 for particles grafted with PEG1000. As seen, for low salt concentrations  $S_{\text{eff}}(q) \approx 1$  indicating negligible correlations. For higher concentrations  $S_{\text{eff}}(q)$  shows an upturn at low  $q$  followed by oscillations. While this behaviour can be captured to some extent using the Debye-Bueche model [88, 89, 90], it involves many parameters. Also, the volume fraction in the MSA calculations must be increased to obtain a reasonable fit. Therefore, we investigated the scattering using a cluster model with direct calculation of the scattering signal.

The effective structure factor of a cluster was calculated as [107]

$$S_{\text{eff}}^{\text{cluster}}(q) = 1 + \frac{2}{N} \sum_{i < j}^N \frac{\sin(qr_{ij})}{qr_{ij}} \quad (4.6)$$

where  $r_{ij}$  is the interparticle distance between sphere  $i$  and  $j$ . The positions of the individual spheres in the cluster were calculated by trial-and-error where the  $N$  spheres were randomly moved around in a series of moves that lowered the deviation from the experimental  $S_{\text{eff}}(q)$  data. The effective structure factor for isolated sphere doublets of individual diameter  $\sigma$  can be calculated analytically [107],

$$S_{\text{eff}}(q) = 1 + \frac{\sin(q\sigma)}{q\sigma} \quad (4.7)$$

It gives good agreement with the 0.6 M data in figure 4.11 when  $\sigma = 155$  nm. At higher salt concentrations, the average cluster is larger and the calculation must be done by a computer. The low- $q$  limit of  $S_{\text{eff}}(q)$  is equal to the aggregation number of the cluster [108, 109]. The agreement with the 0.7 M data is obtained for a 40-sphere cluster. Moreover, in this fit the contact distance between spheres,  $\sigma$ , is reduced to 151 nm. This indicates a contraction of the PEG-layer, of a similar order of magnitude as seen in earlier TEM-studies [91]. For the 0.7 M data in figure 4.11, the result was different clusters with a radius of gyration of around 340 nm.

In the work done in Papers I-III, SAXS and SANS measurements were performed at low  $q$ -values, corresponding to large length scales. In Paper IV, we consider a wider range of  $q$ -values and study two different salts,  $\text{Na}_2\text{CO}_3$  and  $\text{Na}_2\text{WO}_4$ , added to dispersions of particles grafted with mPEGA2000. The results are seen in figure 4.12. The slow decay (slower than  $q^{-4}$ ) at large  $q$  indicates a rough particle surface from the grafted polymer [78]. For ideal free PEG-chains the decay is  $q^{-2}$  [8].

Even though  $\text{Na}_2\text{CO}_3$  and  $\text{Na}_2\text{WO}_4$  show similar salting-out behavior for free PEG [110], we see some important differences for the PEG-grafted particles. When extending the  $q$ -region of interest to include larger  $q$ -values, a slight maximum is seen at around  $q \sim 0.8 \text{ nm}^{-1}$  for particles without added salt and with some added  $\text{Na}_2\text{CO}_3$ . A similar maximum is found with added  $\text{Na}_3\text{WO}_4$  but the maximum appears at  $q \sim 0.9 \text{ nm}^{-1}$  for  $\text{Na}_2\text{WO}_4$ . In the case of  $\text{Na}_2\text{CO}_3$ , this  $q$ -value, via  $2\pi/q$ , corresponds well to the thickness of the PEG-layer obtained from TEM-analysis [91]. At 0.5 M of  $\text{Na}_2\text{CO}_3$  this intensity maximum has vanished, correlating well to the earlier observations of the PEG-layer contraction [104, 91].

For the particles with  $\text{Na}_2\text{WO}_4$  there is first a broad intensity increase in the larger  $q$ -range at about  $0.4 - 0.6 \text{ nm}^{-1}$  followed by a similar maximum as for the  $\text{Na}_2\text{CO}_3$  case but at a larger  $q$ -value of  $\sim 0.9 \text{ nm}^{-1}$ . As for the  $\text{Na}_2\text{CO}_3$  series, this second maximum disappears when clusters are formed which in this case happens at a concentration of 0.4 M.

The 0.5 M  $\text{Na}_2\text{CO}_3$  data have been fitted with a sphere form factor using a double shell and can be seen as the solid line in figure 4.12. In order to give the right decay in the high- $q$  region, the shells had to be modeled with an electron contrast lower than that of the surrounding medium. This finding can be attributed to an absence of solvation water in the densely grafted PEG layer. This is supported by computer simulations on planar PEG brushes [94] and it

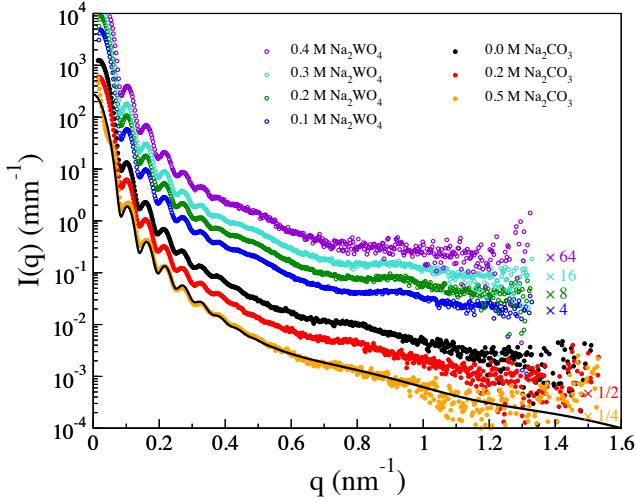


Figure 4.12: The intensity as a function of the scattering vector for particles grafted with mPEGA2000 in the presence of two different salts:  $\text{Na}_2\text{WO}_4$  (upper set) and  $\text{Na}_2\text{CO}_3$  (lower set). The intensities have been shifted for clarity as indicated. The solid line is a model fit.

would also be consistent with the Flory-Huggins model in Paper II. The low contrast could also arise from ion depletion near the PEG layer. Unfortunately, we have not been able to find a model that captures the slight intensity maxima at high  $q$ . Therefore we have not been able to use modeling to quantify the PEG dehydration and possible ion depletion.



## Chapter 5

# Conclusions and future work

In this work, a semi-batch emulsion polymerization method, developed previously [26] for the production of sterically stabilized dispersions, has been extended to allow grafts of different lengths as well as crosslinked particle cores. The synthesis method has also been used for polystyrene cores and a scale up of the synthesis by a factor ten has been achieved. This allows for testing of different theories against the behavior of these model systems for which the usual van der Waals interactions appear insignificant. The crosslinked particles can be transferred to THF and remain stable. Non-crosslinked particles with pHFBMA cores swell uncontrollably in this solvent. Therefore, these particles can also be used in non-aqueous solvents without losing their integrity.

For the first time, we are able to report that a sterically stabilized system with shorter polymer grafts leads to greater stability than one with longer grafts. Since this has not been reported before, this experimental finding presumably requires a vanishing contribution from van der Waals core-core interactions, which is expected for these particles with fluorinated cores. The effect of the shell thickness is very strong. For HFBMA particles grafted with mEGA130, the dispersions remain stable against addition of  $\text{Na}_2\text{CO}_3$  even at salt concentrations not much below saturation. On the other hand, HFBMA particles grafted with mPEGA5000 become unstable already at around 0.5-0.6 M  $\text{Na}_2\text{CO}_3$ . It is worth emphasizing that the  $\text{CO}_3^{2-}$  ion is strongly hydrated and particularly effective at salting out particles and macromolecules.  $\text{NaCl}$ , by contrast, is completely ineffective.

Keeping the grafts fixed, dispersions of varying particle concentrations have been tested against sodium carbonate addition in order to determine any effect on the stability. It was found that the stability limit in this case is independent of the particle concentration. This led us to conclude that the instability is due to a “dewetting transition” of the grafted PEG shell and that the free energy of this dewetting transition is independent of the particle concentration; that is, it is a single-particle effect that is triggered when going beyond a salt concentration threshold. Additionally, interpretation of SAXS data showed that permanent clusters are formed above this salt concentration.

In support of the dewetting hypothesis, IFT measurements were performed between toluene and dispersions with varying amounts of salt. The results show that the particles move to the surface spontaneously, even without any added salt, but they migrate to the surface to a larger extent as salt is added. Furthermore, SANS measurements revealed a decrease in the shell thickness just as the particles become unstable from adding sodium carbonate. The sodium carbonate stability limit for different lengths of the grafted mPEGA is captured by a Flory-Huggins parameter-based equation where the Flory-Huggins parameter of the polymer graft is taken as a weighted average of repeating and terminal parts of the grafted chain.

While some initial steps have been made in order to achieve a better understanding of the mechanism behind sterically stabilized particles going from a stable to an unstable state, more work is needed in order to fully understand the mechanism. In this work, it was shown that the mPEGA2000-grafted HF-BMA particles are interfacial active at the water-toluene interface. It is likely the case for the surface tension (water-air) as well. Creaming has been seen occasionally for these particles [91]. A more extensive investigation of the phase behaviour of the dispersions is called for. This typically requires relatively large quantities of dispersion but Bleier and coworkers [111] have developed a microfluidic droplet-based method where much smaller quantities are needed for a well-covered phase behavior study. This method may possibly be used for these studies as it has been successfully applied to solutions of free PEG.

To achieve a greater understanding of the surface activity effect, grazing incidence small angle X-ray scattering (GISAXS) could be employed for further investigations of the surface structure and specular X-ray reflectivity (SXRR) could be used to investigate potential ion depletion at the surface. Both these methods have been previously used for dispersions of PEG-grafted gold nanoparticles [24].

Even though we have strong indications that the surface coverage of PEG is high on the particle surface [26], it would be valuable to be able to quantify this. One way could be to exchange the methyl end-group for a titratable one, such as -OH. The PEG synthesis scheme has been shown to work well with changes already. However, care has to be taken so that all unreacted PEG is removed, which has been seen in the IFT studies to be difficult. The advantage of targeting the end group only is that it is likely to be accessible from the solvent. Similar methods have been focused on complexation with ether oxygens on PEG [112], but many of these groups may be less accessible. Other possible techniques to determine the surface coverage could be nuclear magnetic resonance (NMR) and thermogravimetric analysis (TGA) which have been employed to quantify the grafting density of PEG on lipid [113] and gold [22, 114] nanoparticles, respectively.

# Acknowledgments

First, I would like to express my greatest appreciation for my supervisor, **Johan Bergenholtz**, your knowledge and positive attitude to science are inspiring. Thank you for always taking the time to explain and discuss when needed and proof-reading and providing writing suggestions for my thesis.

I would also like to thank my examiner, **Gunnar Nyman**, for the valuable conversations about aspects beyond the scientific part of my project.

I thank the present and past members and guests of the Physical Chemistry group for all the conversations and social activities. A special thanks goes to **Karl-Mikael Svensson** – for being my friend and colleague all the way from our undergraduate studies up to this day; we have made this journey together – to **Daria Burdakova** – for always bringing a smile and positive energy wherever you go – to **Ignacio Suárez Martín** – for your open mind and for sharing Spanish culture – and to **Rasoul Hashemi** – for all the encouragements.

I want to acknowledge my co-authors, **Jeanette Ulama** for your guidance and help when taking over this project from you; **Malin Johansson** – it has been a great pleasure to be working with you for both your bachelor and master thesis projects, tackling both new experimental techniques and results together; **Malin Zackrisson Oskolkova** for the help with the SAXS measurements in Lund and at the ESRF; **Theyengeri Narayana** and **Michael Sztucki** for all the help at the ESRF; **Grethe Vestergaard Jensen** for the possibility to go to NIST and for all the help with the SANS measurements; **Romain Bordes**, for all your experimental help as well as valuable discussions during the surface active particles part of this project. I also wish to acknowledge **Lynn Walker** and **Michael Davidson** for the warm welcome in your group and lab during the days I spent there.

To my family, **Mamma, Pappa, Linnea** och **Johan** för allt stöd och all uppmuntran jag fått under alla år: det har betytt väldigt mycket. To my nephews, **Alvar** och **Eje**, tack för att ni ger mig en paus när vi träffas, ni är fantastiska! To **Rasmus** for all the support you have provided for many years, for always being enthusiastic to talk about “my stuff” regardless if its English grammar, thermodynamics or just how life is as a PhD student. Being a co-author with you in one of the papers turned out to be a great experience where we both could share our expertise. I’m also grateful for your encouragement and support during the writing process of this thesis, and for proof-reading it.



# Bibliography

- [1] P. N. Pusey and W. Van Megen. Phase behaviour of concentrated suspensions of nearly hard colloidal spheres. *Nature*, 320(6060):340–342, 1986.
- [2] J-D. Lee, J-H. So, and S-M. Yang. Rheological behavior and stability of concentrated silica suspensions. *J. Rheol.*, 43(5):1117–1140, 1999.
- [3] K. N. Pham, A. M. Puertas, J. Bergenholtz, S. U. Egelhaaf, A. Moussaid, P. N. Pusey, A. B. Schofield, M. E. Cates, M. Fuchs, and W. C. K. Poon. Multiple glassy states in a simple model system. *Science*, 296(5565):104–106, 2002.
- [4] V. J. Anderson and H. N. W. Lekkerkerker. Insights into phase transition kinetics from colloid science. *Nature*, 416(6883):811, 2002.
- [5] W. Härtl, H. Versmold, U. Wittig, and P. Linse. Structure and dynamics of polymer colloid suspensions from dynamic light scattering and brownian dynamics simulation. *J. Chem. Phys.*, 97(10):7797–7804, 1992.
- [6] R. Krause, G. Nägele, D. Karrer, J. Schneider, R. Klein, and R. Weber. Structure and self-diffusion in dilute suspensions of polystyrene spheres: experiment vs. computer simulation and theory. *Phys. A*, 153(3):400–419, 1988.
- [7] Y. Monovoukas and A. P. Gast. The experimental phase diagram of charged colloidal suspensions. *J. Colloid Interface Sci.*, 128(2):533–548, 1989.
- [8] P. G. De Gennes. Polymers at an interface; a simplified view. *Adv. Colloid Interface Sci.*, 27(3-4):189–209, 1987.
- [9] Y. Liang, N. Hilal, P. Langston, and V. Starov. Interaction forces between colloidal particles in liquid: Theory and experiment. *Adv. Colloid Interface Sci.*, 134:151–166, 2007.
- [10] F. T. Hesslink, A. Vrij, and J. T. G Overbeek. Theory of the stabilization of dispersions by adsorbed macromolecules. ii. interaction between two flat particles. *J. Phys. Chem.*, 75(14):2094–2103, 1971.

- [11] A. Vrij. Polymers at interfaces and the interactions in colloidal dispersions. *Pure Appl. Chem.*, 48(4):471–483, 1976.
- [12] D. H. Napper. Steric stabilization. *J. Colloid Interface Sci.*, 58(2):390–407, 1977.
- [13] G. Rossi and P. A. Pincus. Interactions between unsaturated-polymer adsorbed surfaces. *EPL (Europhys. Lett.)*, 5(7):641, 1988.
- [14] P. G. De Gennes. Stabilité de films polymère/solvant. *Comptes rendus de l'Académie des sciences. Série 2, Mécanique, Physique, Chimie, Sciences de l'univers, Sciences de la Terre*, 300(17):839–843, 1985.
- [15] J. N. Israelachvili, M. Tirrell, J. Klein, and Y. Almog. Forces between two layers of adsorbed polystyrene immersed in cyclohexane below and above the  $\theta$  temperature. *Macromolecules*, 17(2):204–209, 1984.
- [16] J. W. Jansen, C. G. De Kruif, and A. Vrij. Attractions in sterically stabilized silica dispersions: II. experiments on phase separation induced by temperature variation. *J. Colloid Interface Sci.*, 114(2):481–491, 1986.
- [17] R. C. Kramb and C. F. Zukoski. A metastable van der waals gel: Transitioning from weak to strong attractions. *Langmuir*, 24(14):7565–7572, 2008.
- [18] M. A. Bevan and P. J. Scales. Solvent quality dependent interactions and phase behavior of polystyrene particles with physisorbed peo- ppo- peo. *Langmuir*, 18(5):1474–1484, 2002.
- [19] S. Roke, J. Buitenhuis, J. C. Van Miltenburg, M. Bonn, and A. van Blaaderen. Interface–solvent effects during colloidal phase transitions. *J. Phys.: Condens. Matter*, 17(45):S3469, 2005.
- [20] S. Roke, O. Berg, J. Buitenhuis, A. van Blaaderen, and M. Bonn. Surface molecular view of colloidal gelation. *Proc. Nat. Acad. Sci.*, 103(36):13310–13314, 2006.
- [21] H. Zhang, W. Wang, S. Mallapragada, A. Travesset, and D. Vaknin. Ion-specific interfacial crystallization of polymer-grafted nanoparticles. *J. Phys. Chem. C*, 121(28):15424–15429, 2017.
- [22] H. Zhang, W. Wang, S. Mallapragada, A. Travesset, and D. Vaknin. Macroscopic and tunable nanoparticle superlattices. *Nanoscale*, 9(1):164–171, 2017.
- [23] H. Zhang, W. Wang, M. Akinc, S. Mallapragada, A. Travesset, and D. Vaknin. Assembling and ordering polymer-grafted nanoparticles in three dimensions. *Nanoscale*, 9(25):8710–8715, 2017.

- 
- [24] W. Wang, H. Zhang, S. Mallapragada, A. Travesset, and D. Vaknin. Ionic depletion at the crystalline gibbs layer of peg-capped gold nanoparticle brushes at aqueous surfaces. *Phys. Rev. Mater.*, 1(7):076002, 2017.
- [25] T. López-León, A. B. Jódar-Reyes, D. Bastos-González, and J. L. Ortega-Vinuesa. Hofmeister effects in the stability and electrophoretic mobility of polystyrene latex particles. *J. Phys. Chem. B*, 107(24):5696–5708, 2003.
- [26] J. Ulama, M. Zackrisson Oskolkova, and J. Bergenholtz. Monodisperse pegylated spheres: an aqueous colloidal model system. *J. Phys. Chem. B*, 118(9):2582–2588, 2014.
- [27] P. Lo Nostro and B. W. Ninham. Hofmeister phenomena: an update on ion specificity in biology. *Chem. Rev.*, 112(4):2286–2322, 2012.
- [28] J. M. Harris. *Poly (ethylene glycol) chemistry: biotechnical and biomedical applications*. Springer Science & Business Media, 2013.
- [29] B. Jeong, Y. H. Bae, and S. W. Kim. Drug release from biodegradable injectable thermosensitive hydrogel of peg-plga-peg triblock copolymers. *J. Contr. release*, 63(1-2):155–163, 2000.
- [30] J. R. Lu, T. J. Su, R. K. Thomas, J. Penfold, and R. W. Richards. The determination of segment density profiles of polyethylene oxide layers adsorbed at the air-water interface. *Polymer*, 37:109–114, 1996.
- [31] T. Gilanyi, I. Varga, M. Gilanyi, and R. Meszaros. Adsorption of poly(ethylene oxide) at the air/water interface: a dynamic and static surface tension study. *J. Colloid Interface Sci.*, 301:428–435, 2006.
- [32] K. Ito, B. B. Sauer, R. J. Skarlupka, M. Sano, and H. Yu. Dynamic interfacial properties of poly(ethylene oxide) and polystyrene at toluene/water interface. *Langmuir*, 6(8):1379–1388, 1990.
- [33] M. Spitzer, E. Sabadini, and W. Loh. Poly (ethylene glycol) or poly (ethylene oxide)?: Magnitude of end-group contribution to the partitioning of ethylene oxide oligomers and polymers between water and organic phases. *J. Braz. Chem. Soc.*, 13(1):7–9, 2002.
- [34] E. E. Dormidontova. Influence of end groups on phase behavior and properties of peo in aqueous solutions. *Macromolecules*, 37(20):7747–7761, 2004.
- [35] S. Saeki, N. Kuwahara, M. Nakata, and M. Kaneko. Upper and lower critical solution temperatures in poly (ethylene glycol) solutions. *Polymer*, 17(8):685–689, 1976.
- [36] K. P. Ananthapadmanabhan and E. D. Goddard. Aqueous biphasic formation in polyethylene oxide-inorganic salt systems. *Langmuir*, 3(1):25–31, 1987.

- [37] E. Florin, R. Kjellander, and J. C. Eriksson. Salt effects on the cloud point of the poly (ethylene oxide)+ water system. *J. Chem. Soc., Faraday Trans. 1: Phys. Chem. Condens. Phases*, 80(11):2889–2910, 1984.
- [38] H. S. Frank and M. W. Evans. Free volume and entropy in condensed systems iii. entropy in binary liquid mixtures; partial molal entropy in dilute solutions; structure and thermodynamics in aqueous electrolytes. *J. Chem. Phys.*, 13(11):507–532, 1945.
- [39] D. Urban and K. Takamura. *Polymer dispersions and their industrial applications*. Wiley Online Library, 2002.
- [40] W. D. Harkins. A general theory of the reaction loci in emulsion polymerization. *J. Chem. Phys.*, 13(9):381–382, 1945.
- [41] W. D. Harkins. A general theory of the reaction loci in emulsion polymerization. ii. *J. Chem. Phys.*, 14(1):47–48, 1946.
- [42] W. D. Harkins. A general theory of the mechanism of emulsion polymerization1. *J. Am. Chem. Soc.*, 69(6):1428–1444, 1947.
- [43] W. D. Harkins. General theory of mechanism of emulsion polymerization. ii. *J. Polym. Sci. A: Polym. Chem.*, 5(2):217–251, 1950.
- [44] W. V. Smith and R. H. Ewart. Kinetics of emulsion polymerization. *J. Chem. Phys.*, 16(6):592–599, 1948.
- [45] W. V. Smith. The kinetics of styrene emulsion polymerization1a. *J. Am. Chem. Soc.*, 70(11):3695–3702, 1948.
- [46] W. V. Smith. Chain initiation in styrene emulsion polymerization. *J. Am. Chem. Soc.*, 71(12):4077–4082, 1949.
- [47] F. K. Hansen and J. Ugelstad. Emulsification and emulsion polymerization of styrene using mixtures of cationic surfactant and long chain fatty alcohols or alkanes as emulsifiers. In I. Piirma, editor, *Emulsion polymerization*, chapter 1, pages 1–23. Academic Press, New York, 1976.
- [48] R. M. Fitch and C. H. Tsai. Particle formation in polymer colloids. iii. prediction of the number of particles by a homogeneous nucleation theory, 1971.
- [49] J. W. Vanderhoff. Semi-continuous emulsion polymerization. In M. S. El-Aasser and R. M. Fitch, editors, *Future Directions in Polymer Colloids*, pages 23–45. Springer Netherlands, Dordrecht, 1987.
- [50] W. Härtl and X. Zhang-Heider. The synthesis of a new class of polymer colloids with a low index of refraction. *J. Colloid Interface Sci.*, 185(2):398–401, 1997.

- 
- [51] G. Pan, A. S. Tse, R. Kesavamoorthy, and S. A. Asher. Synthesis of highly fluorinated monodisperse colloids for low refractive index crystalline colloidal arrays. *J. Am. Chem. Soc.*, 120(26):6518–6524, 1998.
- [52] G. H. Koenderink, S. Sacanna, C. Pathmamanoharan, M. Raşa, and A. P. Philipse. Preparation and properties of optically transparent aqueous dispersions of monodisperse fluorinated colloids. *Langmuir*, 17(20):6086–6093, 2001.
- [53] S. Sacanna, G. H. Koenderink, and A. P. Philipse. Microemulsion synthesis of fluorinated latex spheres. *Langmuir*, 20(19):8398–8400, 2004.
- [54] K. Suresh, T. Pakula, and E. Bartsch. Synthesis, morphology and rheological behavior of fluoropolymer-polyacrylate nanocomposites. *Macromol. Reaction Eng.*, 1(2):253–263, 2007.
- [55] W. H. Keesom. On the deduction of the equation of state from boltzmann’s entropy principle’. In *KNAW, Proceedings*, volume 15, pages 240–256, 1912.
- [56] W. H. Keesom. On the second virial coefficient for di-atomic gases. *Koninklijke Nederlandse Akademie van Wetenschappen Proceedings Series B Physical Sciences*, 15:417–431, 1912.
- [57] H. J. Butt, K. Graf, and M. Kappl. *Physics and chemistry of interfaces*. Wiley-VCH, Weinheim, 2003.
- [58] H. C. Hamaker. The london—van der waals attraction between spherical particles. *Physica*, 4(10):1058–1072, 1937.
- [59] F. London. Zur theorie und systematik der molekularkräfte. *Z. Phys. A*, 63(3):245–279, 1930.
- [60] F. London. The general theory of molecular forces. *Trans. Faraday Soc.*, 33:8b–26, 1937.
- [61] J. N. Israelachvili. *Intermolecular and surface forces*. Academic Press, New York, 2011.
- [62] D. F. Evans and H. Wennerström. *Colloidal domain*. Wiley-VCH, Weinheim, 1999.
- [63] J. Mahanty and B. W. Ninham. *Dispersion forces*. Academic Press London, 1976.
- [64] P. C. Hiemenz and R. Rajagopalan. *Principles of Colloid and Surface Chemistry*. CRC Press, Boca Raton, 1997.
- [65] N. V. Churaev, B. V. Derjaguin, and V. M. Muller. *Surface forces*. Plenum Pub Corp, 1987.

- [66] S. Marčelja and N. Radić. Repulsion of interfaces due to boundary water. *Chem. Phys. Lett.*, 42(1):129–130, 1976.
- [67] D. Schiby and E. Ruckenstein. The role of the polarization layers in hydration forces. *Chem. Phys. Lett.*, 95(4-5):435–438, 1983.
- [68] P. Attard and M. T. Batchelor. A mechanism for the hydration force demonstrated in a model system. *Chem. Phys. Lett.*, 149(2):206–211, 1988.
- [69] S. Marčelja. Hydration in electrical double layers. *Nature*, 385(6618):689, 1997.
- [70] J. N. Israelachvili and H. Wennerström. Hydration or steric forces between amphiphilic surfaces? *Langmuir*, 6(4):873–876, 1990.
- [71] D. H. Napper. Modern theories of colloid stability. *Sci. Prog. (1933-)*, pages 91–109, 1967.
- [72] T. R. Briggs. Emulsions with finely divided solids. *Ind. Eng. Chem.*, 13(11):1008–1010, 1921.
- [73] E. H. Lucassen-Reynders and M Tempel, van den Tempel. Stabilization of water-in-oil emulsions by solid particles. *J. Phys. Chem.*, 67(4):731–734, 1963.
- [74] R. Aveyard, B. P. Binks, and J. H. Clint. Emulsions stabilised solely by colloidal particles. *Adv. Colloid Interface Sci.*, 100:503–546, 2003.
- [75] L. Isa, E. Amstad, K. Schwenke, E. Del Gado, P. Ilg, M. Kröger, and E. Reimhult. Adsorption of core-shell nanoparticles at liquid–liquid interfaces. *Soft Matter*, 7(17):7663–7675, 2011.
- [76] P. N. Pusey. Dynamic light scattering. In P. Lindner and T. Zemb, editors, *Neutrons, X-rays and Light: Scattering Methods Applied to Soft Condensed Matter*, chapter 9, pages 203–220. North-Holland, Amsterdam, 2002.
- [77] B. J. Berne and R. Pecora. *Dynamic light scattering: with applications to chemistry, biology, and physics*. Courier Corporation, 2000.
- [78] O. Spalla. General theorems in small-angle scattering. In P. Lindner and T. Zemb, editors, *Neutrons, X-rays and Light: Scattering Methods Applied to Soft Condensed Matter*, chapter 3, pages 49–71. North-Holland, Amsterdam, 2002.
- [79] I. M. Watt. *The principles and practice of electron microscopy*. Cambridge University Press, 1997.
- [80] W. Kühlbrandt. Microscopy: cryo-EM enters a new era. *Elife*, 3:e03678, 2014.

- 
- [81] J. Kuntsche, J. C. Horst, and H. Bunjes. Cryogenic transmission electron microscopy (cryo-tem) for studying the morphology of colloidal drug delivery systems. *Int. J. Pharmaceutics*, 417(1):120–137, 2011.
- [82] R. M. Fitch. *Polymer colloids: A comprehensive introduction*. Academic Press, 1997.
- [83] R. Garcia-Diez, A. Sikora, C. Gollwitzer, C. Minelli, and M. Krumrey. Simultaneous size and density determination of polymeric colloids by continuous contrast variation in small angle x-ray scattering. *Eur. Polym. J.*, 81:641–649, 2016.
- [84] T. Allen. *Powder sampling and particle size determination*. Elsevier, 2003.
- [85] D. B. Thiessen, D. J. Chione, C. B. McCreary, and W. B. Krantz. Robust digital image analysis of pendant drop shapes. *J. Colloid Interface Sci.*, 177(2):658–665, 1996.
- [86] H. C. Lichstein and M. H. Soule. Studies of the effect of sodium azide on microbic growth and respiration: I. the action of sodium azide on microbic growth. *J. Bacteriol.*, 47(3):221, 1944.
- [87] M. Kotlarchyk and S-H. Chen. Analysis of small angle neutron scattering spectra from polydisperse interacting colloids. *J. Chem. Phys.*, 79(5):2461–2469, 1983.
- [88] D. Pontoni, T. Narayanan, J-M. Petit, G. Grübel, and D. Beysens. Microstructure and dynamics near an attractive colloidal glass transition. *Phys. Rev. Lett.*, 90(18):188301, 2003.
- [89] A. Muratov, A. Moussaid, T. Narayanan, and E. Kats. A percus-yevick description of the microstructure of short-range interacting metastable colloidal suspensions. *J. Chem. Phys.*, 131(5):054902, 2009.
- [90] P. Debye and A. M. Bueche. Scattering by an inhomogeneous solid. *J. Appl. Phys.*, 20(6):518–525, 1949.
- [91] J. Ulama, M. Zackrisson Oskolkova, and J. Bergenholtz. Polymer-graft-mediated interactions between colloidal spheres. *Langmuir*, 32(12):2882–2890, 2016.
- [92] E. Waisman. The radial distribution function for a fluid of hard spheres at high densities: mean spherical integral equation approach. *Molecular Phys.*, 25(1):45–48, 1973.
- [93] P. T. Cummings and E. R. Smith. Liquid—gas transition for hard spheres with attractive yukawa tail interactions. *Chem. Phys.*, 42(3):241–247, 1979.

- [94] U. Dahal, Z. Wang, and E. E. Dormidontova. Hydration of spherical peo-grafted gold nanoparticles: Curvature and grafting density effect. *Macromolecules*, 51(15):5950–5961, 2018.
- [95] L. Isa, E. Amstad, K. Schwenke, E. del Gado, P. Ilg, M. Kroger, and E. Reimhult. Adsorption of core-shell nanoparticles at liquid-liquid interfaces. *Soft Matter*, 7:7663–7675, 2011.
- [96] L. Isa, D. C. E. Calzolari, D. Pontoni, T. Gillich, A. Nelson, R. Zirbs, A. Sanchez-Ferrer, R. Mezzenga, and E. Reimhult. Core-shell nanoparticle monolayers at planar liquid-liquid interfaces: effects of polymer architecture on the interface microstructure. *Soft Matter*, 9:3789–3797, 2013.
- [97] A. Nelson, D. Wang, K. Koynov, and L. Isa. A multiscale approach to the adsorption of core-shell nanoparticles at fluid interfaces. *Soft Matter*, 11:118–129, 2015.
- [98] S. M. S. Björkegren, L. Nordstierna, A. Törncrena, M. E. Persson, and A. E. C. Palmqvist. Surface activity and flocculation behavior of polyethylene glycol-functionalized silica nanoparticles. *J. Colloid Interface Sci.*, 452:215–223, 2015.
- [99] K. Schwenke, L. Isa, D. L. Cheung, and E. del Gado. Conformations and effective interactions of polymer-coated nanoparticles at liquid interfaces. *Langmuir*, 30:12578–12586, 2014.
- [100] X. Yong. Modeling the assembly of polymer-grafted nanoparticles at oil-water interfaces. *Langmuir*, 31:11458–11469, 2015.
- [101] P. Schurtenberger. Contrast and contrast variation in neutron, x-ray and light scattering. In Lindner P. and T. Zemb, editors, *Neutrons, X-rays and Light: Scattering Methods Applied to Soft Condensed matter*. North-Holland, 2002.
- [102] C. Branca, A. Faraone, S. Magazu, G. Maisano, P. Migliardo, A. Triolo, R. Triolo, and V. Villari. Anomalous conformational properties of peo in h<sub>2</sub>o and d<sub>2</sub>o by sans, pcs and raman scattering. *J. Appl. Cryst.*, 33(3):709–713, 2000.
- [103] C. Branca, A. Faraone, G. Maisano, S. Magazu, P. Migliardo, A. Triolo, R. Triolo, and V. Villari. Can the isotopic hd substitution affect the conformational properties of polymeric aqueous solutions? the poly (ethylene oxide)-water case. *J. Phys.: Condens. Matter*, 11(32):6079, 1999.
- [104] G. K. Jonsson, J. Ulama, R. A. X. Persson, M. Zackrisson Oskolkova, M. Sztucki, T. Narayanan, and J. Bergenholtz. Stabilizing colloidal particles against salting-out by shortening surface grafts. *Langmuir*, 35:11836–11842, 2019.

- 
- [105] F. E. Bailey and J. V. Koleske. *Poly(ethylene oxide)*. Academic Press, New York, 1976.
- [106] P. Raffa, A. A. Broekhuis, and F. Picchioni. Amphiphilic copolymers based on peg-acrylate as surface active water viscosifiers: Towards new potential systems for enhanced oil recovery. *J. Appl. Polym. Sci.*, 133(42), 2016.
- [107] P. Debye. Zerstreung von röntgenstrahlen. *Ann. Phys.*, 351(6):809–823, 1915.
- [108] W. Li, B. A. Persson, M. Lund, J. Bergenholtz, and M. Zackrisson Oskolkova. Concentration-induced association in a protein system caused by a highly directional patch attraction. *J. Phys. Chem. B*, 120(34):8953–8959, 2016.
- [109] Y. V. Kalyuzhnyi, M. F. Holovko, and A. D. J. Haymet. Integral equation theory for associating liquids: Weakly associating 2–2 electrolytes. *J. Chem. Phys.*, 95(12):9151–9164, 1991.
- [110] R. Sadeghi and R. Golabiazar. Thermodynamics of phase equilibria of aqueous poly (ethylene glycol)+ sodium tungstate two-phase systems. *J. Chem. Eng. Data*, 55(1):74–79, 2009.
- [111] B. J. Bleier, S. L. Anna, and L. M. Walker. Microfluidic droplet-based tool to determine phase behavior of a fluid system with high composition resolution. *J. Phys. Chem. B*, 122(14):4067–4076, 2018.
- [112] M. C. L. Maste, A. P. C. M. van Velthoven, W. Norde, and J. Lyklema. Synthesis and characterization of a short-haired poly (ethylene oxide)-grafted polystyrene latex. *Colloids Surf. A Physicochem. Eng. Asp.*, 83(3):255–260, 1994.
- [113] M. Garcia-Fuentes, D. Torres, M. Martín-Pastor, and M. J. Alonso. Application of nmr spectroscopy to the characterization of peg-stabilized lipid nanoparticles. *Langmuir*, 20(20):8839–8845, 2004.
- [114] D. N. Benoit, H. Zhu, M. H. Lilierose, R. A. Verm, N. Ali, A. N. Morrison, J. D. Fortner, C. Avendano, and V. L. Colvin. Measuring the grafting density of nanoparticles in solution by analytical ultracentrifugation and total organic carbon analysis. *Anal. Chem.*, 84(21):9238–9245, 2012.